## ABSTRACT

## AUTOMATIC REGISTRATION AND SEGMENTATION OF ABDOMINAL IMAGES AND DETECTION OF PANCREATIC CANCER

**by**
**Girish Kumar Maniprasad**

Localized and detailed analyses of 3D abdominal images obtained through different imaging modalities help greatly in determining the progression of a disease or for post-operative treatment / evaluation. However, such analyses become difficult and sometimes unfeasible due to the effects of patient motion and breathing. This is particularly evident during analysis of the pancreas for cancer, due to its proximity to other intra-abdominal organs. Within subject registration thus becomes imperative for pathological analysis of pancreatic cancer. An intensity-based, global image registration algorithm was developed in the present work, for registration of pancreatic abdominal images. The registration algorithm was automatic and could register three dimensional MR and CT images of the abdomen. Once registered, localization and analysis of the pancreas was facilitated by a semi-automatic k-means clustering based segmentation procedure. Such a registration and segmentation based method could be used as a valuable tool for pancreas cancer screening and analysis.

# AUTOMATIC REGISTRATION AND SEGMENTATION OF ABDOMINAL IMAGES AND DETECTION OF PANCREATIC CANCER

by
**Girish Kumar Maniprasad**

**A Thesis**
**Submitted to the Faculty of**
**New Jersey Institute of Technology**
**in Partial Fulfillment of the Requirements for the Degree of**
**Master of Science in Biomedical Engineering**

**Department of Biomedical Engineering**

**May 2007**

## APPROVAL SHEET

# AUTOMATIC REGISTRATION AND SEGMENTATION OF ABDOMINAL IMAGES AND DETECTION OF PANCREATIC CANCER

**Girish Kumar Maniprasad**

---

Dr. Bharat B. Biswal, Thesis Advisor — Date
Associate Professor of Radiology, UMDNJ

---

Dr. Richard A. Foulds, Thesis Co-advisor — Date
Associate Professor of Biomedical Engineering, NJIT

Dr. Tara L. Alvarez, Committee Member — Date
Associate Professor of Biomedical Engineering, NJIT

## BIOGRAPHICAL SKETCH

**Author:** Girish Kumar Maniprasad

**Degree:** Master of Science

**Date:** May 2007

**Major:** Biomedical Engineering

**Graduate and Undergraduate Education:**

- Master of Science in Biomedical Engineering,
  New Jersey Institute of Technology, Newark, NJ, 2007

- Bachelor of Engineering in Electrical and Electronics Engineering
  Anna University, Chennai, India, 2005

**Poster Presentation:**

Girish K. Maniprasad, Nirvish Shah, Bharat B. Biswal,
"Automatic Registration and Segmentation of Pancreatic Images",
The Fifteenth Joint Annual ISMRM-ESMRMB Meeting,
Berlin, Germany, 19-25 May 2007.

To all the people who made this endeavor possible

## ACKNOWLEDGMENT

First of all, I would like to express my heartfelt thanks and deepest gratitude to my mentor Dr. Bharat Biswal who guided me throughout this project and was available at all times, providing me with valuable information and innumerable resources. Without his constant presence and support, this thesis work would not have been possible. My sincere thanks to Dr. Richard Foulds for his valuable and timely advice in the initial stages, which have contributed towards the success of my thesis. Special thanks to Dr. Tara Alvarez for agreeing to be my third committee and presiding over my defense.

I would also like to thank the Radiology Department of the University of Medicine and Dentistry of New Jersey for their financial and technical support.

I also wish to thank Nirvish Shah for his invaluable time and for enlightening me with valuable information during our numerous discussions. Many thanks to all my family members, close friends and peers for their emotional support and encouragement.

Last but not least, I would like to thank NJIT for providing me with this opportunity of doing such a good research in the field of Medical Image Processing.

## TABLE OF CONTENTS

## TABLE OF CONTENTS
## (Continued)

## LIST OF TABLES

## LIST OF FIGURES

## LIST OF FIGURES
## (Continued)

## LIST OF FIGURES
## (Continued)

# CHAPTER 1

# INTRODUCTION

## 1.1 Objective

The primary objective of this thesis project was to implement and evaluate image registration and segmentation of pancreatic images obtained using single as well as multiple modalities (CT and MRI). Once such a method was developed, the next step was to illustrate the application of such a processing tool in the early detection of pancreatic cancer.

## 1.2 The Human Abdomen and the Pancreas

The anatomical location of the human abdomen is between the thoracic diaphragm (below the lungs) and the pelvic brim (the notch atop the pelvis). The abdominal cavity houses organs of the digestive tract, the liver, the pancreas, the kidneys and the spleen. It also contains numerous blood vessels including the inferior vena cava and the aorta. The entire abdominal cavity is encompassed by the abdominal wall which is divided as the anterior wall, the posterior wall and the lateral walls respectively [1].

The pancreas is an important organ that lies transverse (parallel to the ground when person is upright) in the posterior abdomen, behind the stomach region. It secretes the pancreatic digestive juices and produces important hormones such as insulin thus functioning as an exocrine as well as an endocrine organ. The pancreas is further subdivided into three main regions viz., the head, the body and the tail. The head of the pancreas is a bulky structure lying close to the duodenum. The body is the structure following the head lying near the spine and bordering the stomach. The tail is an

elongated structure extending towards the spleen [1, 2]. A typical image illustrating the location of the pancreas is as shown below:

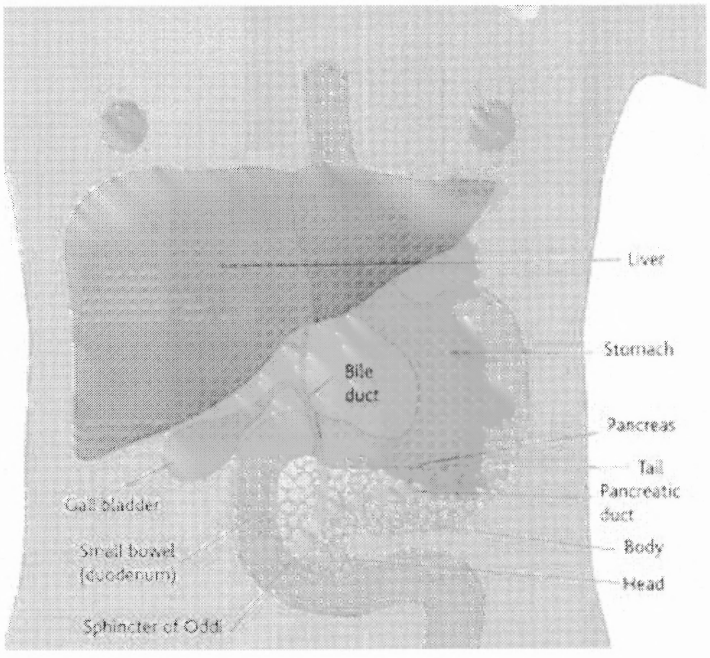


**Figure 1.1** Location and regions of the pancreas. [34]

### 1.2.1 Imaging of the Abdomen and Pancreas

Images of the abdomen are typically acquired while the patient lies in a supine position inside the scanner. A sequential set of images covering the abdomen is then obtained in a rapid fashion. Typically, subjects are instructed to hold their breath for short periods of time (between 20 – 50 seconds) while images are being acquired. This method thus provides a significant challenge for high resolution anatomical imaging of the abdomen and the intra abdominal organs. Thus, the number of sequential images and the spatial resolution that can be acquired through the imaging modality is limited not by the physics but by the underlying physiology. Depending on the requirements, an axial (cross-

sectional) view, a longitudinal (lengthwise) view or a sagittal (side) view of the abdomen can be obtained by imaging.

Each of the sequential images obtained on scanning the entire abdomen represent a fractional region of the abdomen and is called as a slice. Slices can be assumed as 2D images with small but significant thickness. Each successive slice is then stacked or grouped to form the entire abdominal region and this is referred to as a volume image. Such volume images are digitally represented by a three dimensional spatial grid where each point is called as a *voxel* (similar to a pixel or picture element in a 2D image). Each voxel value corresponds to the image intensity value at a particular point in the 3D spatial grid representing the entire volume image. A cross-sectional (axial) slice of the abdomen and its various organs as obtained by a CT scan is illustrated in the Figure 1.2 shown below:

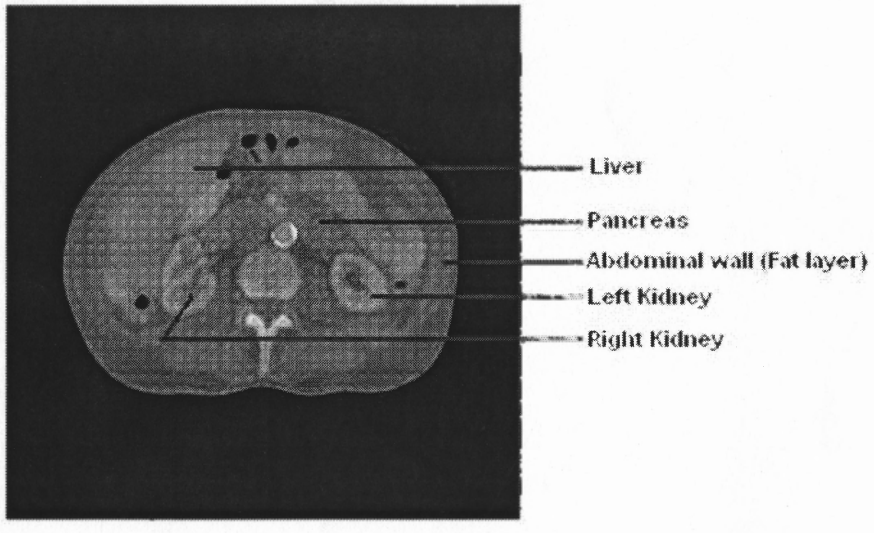


**Figure 1.2** An axial CT slice of the human abdomen.

Each slice is represented by a 2D matrix of intensity values. Resolution of the image slice is governed by the number of rows and columns of this matrix and is always in powers of two. An image with 512 rows and 512 columns or a resolution of 512 x 512 displays more detail about the region than an image with a resolution of 256 x 256. A 3D volume is a group of 2D slices and is thus represented by a three-dimensional matrix. Resolution of a 3D image volume is governed by the number of rows and columns in the individual slices as well as the slice thickness.

Developing an effective imaging procedure that depicts all the organs in the abdomen with intricate details has always been difficult. This difficulty is primarily due to the non-rigid nature of the abdomen. In other words, unlike the brain which is enclosed inside a rigid cranium, the abdomen has no exoskeleton but only an elastic layer of fat enclosing the intra-abdominal organs. Due to this, the breathing cycle greatly influences the motion of the abdomen during the imaging procedure in addition to the patient movement. Hence, image processing procedures that minimize the effect of such motion in the abdomen images become imperative for further analysis of the imaged volumes.

Recent developments in digital imaging modalities, particularly Magnetic Resonance Imaging (MRI) and Computed Tomography (CT) imaging, have resulted in detailed imaging of the intra-abdominal organs, especially the pancreas [3].

### 1.2.2 Magnetic Resonance Imaging of Pancreas

Magnetic Resonance Imaging (MRI) is a non-invasive procedure of imaging the internal details of the human body. This imaging procedure uses the concept of Nuclear Magnetic Resonance (NMR) to generate an energy signal in the radio frequency range of the electromagnetic spectrum. The image is ultimately generated by reconstruction using the

emitted radiations. Gradient coils and radio frequency coils are used to obtain different orientations of the regions to be imaged and to adjust the image contrast respectively. The strength of the magnetic field applied is measured in Tesla, and 1 Tesla is approximately equal to 30,000 times the magnetic field of the earth.

MR imaging of the pancreas is done using a 1.5 Tesla scanner with phased-array torso coils for improved SNR. Fast spin echo or gradient echo sequences with echo planar imaging are generally used for breath-hold acquisitions of abdominal images. Fat-suppressed, high resolution T1 weighted protocol with injection of a contrast agent is used for more precise detection of pancreatic masses [3].

### 1.2.3 Computed Tomography Imaging of Pancreas

Imaging via Computed Tomography (or Computed Axial Tomography) involves using X-rays to generate a series of 2D images of the region of interest. The series images are then reconstructed using a mathematical reconstruction algorithm to produce a 3D view of the region. CT scanners use a set of X-ray emitters and detectors that are arranged in a circular fashion, in parallel to each other encompassing the region to be imaged. Each detector thus produces a respective 2D X-ray image. Scanning is done with or without contrast agents depending on the requirements.

Multi-detector CT technology with dual phase imaging is generally used for imaging the pancreas in the abdomen, in recent times. Image reconstruction is then done by multi-planar 3D techniques such as volume rendering, maximum intensity projection and shaded surface display reconstruction thus resulting in sharp images of the intra-abdominal organs [3].

## 1.3 Pancreatic Cancer

Cancer in the pancreas is a highly lethal disease that has resulted in high mortality rates in the recent years [2, 4]. If detected in its early stages, the canceraceous tissues can be completely removed through surgery. However, the difficulties in early detection of the cancer, due to non-specific symptoms, have contributed greatly to the delays in diagnosis and treatment of the cancer [4]. Research has also shown that the effects of chemotherapy and radiotherapy on the cancer cells are very feeble [3]. Such therapeutic treatments also result in significant toxicity in most of the cases [2, 3].

Majority of the pancreatic carcinoma is due to adenocarcinoma occurring in the exocrine pancreas more clearly in the ductal epithelium. The exocrine pancreatic carcinomas arise in the proximal part with about 30% of the cancer affecting the body and tail of the pancreas [2, 4]. Another detectable sign of pancreas cancer occurrence is an abnormal enlargement of certain regions of the pancreas due to the initial onset of the cancer causing tissues [2]. Initial symptoms include anorexia, weight loss, abdominal discomfort or pain, and nausea. Most cases have also exhibited jaundice as a symptom for pancreas cancer onset typically from compression of the common duct in the head of the pancreas [2].

Due to the proximity of pancreas to multiple organs and tissues in the abdomen, invasion and propagation of cancer cells to neighboring regions is inevitable. Hence, surgical removal of lesions becomes virtually impossible beyond a certain stage of cancer onset, thus making the disease fatal. Screening of pancreatic cancer using serologic cancer markers also has lost its reliability in the past years. Curative methods such as radiotherapy, chemotherapy and laparoscopy have very little effect on the cancer tissue

beyond a certain stage. Pancreas cancer is becoming one of the most fatal gastrointestinal malignancies having less than a 5% survival of 5 years [4].

The advent of sophisticated diagnostic imaging methods has offered promising results for early cancer detection and treatment [3, 4]. MR and CT imaging modalities help to a great extent in determination of progression of the cancer and treatment evaluation. CT imaging results in thinner image slices with intricate details in each slice. MRI on the other hand is sensitive to the various organ tissues inside the abdomen and hence can distinguish the independent organs in the abdomen more clearly (better spatial resolution) compared to the CT images. Hence if the pancreatic images of a patient obtained through both these modalities are aligned or *registered*, a great deal of information can be inferred. Further, on segmenting the pancreatic region from the abdomen, it can be screened effectively for the presence of cancer or for treatment evaluation. Alignment of the inter-modality images can be facilitated by a suitable image registration method and sectioning out the region of interest for analysis can be done using a corresponding image segmentation procedure.

## 1.4 Methodology – Overview

Medical image registration is the process of matching or aligning two (or more) radiological images representing the same regions of the body. The images to be registered can be similar images obtained from two different imaging modalities (inter-modality) or images obtained from the same modality (intra-modality) that were imaged at different points of time. Optimal information regarding the medical condition of a

patient can thus be obtained if all such images are spatially aligned. Most of the image registration algorithms involve 2D (slices) or 3D (volume) images [5].

Medical image registration can be performed using extrinsic or intrinsic image properties [6]. Extrinsic image registration involves using markers to identify certain anatomically important landmarks and then registering the images based on the location of these markers. Registration performed using intrinsic properties of images can broadly be classified into (a) intensity-based [7-10] and (b) feature-based [11-14] methods. Intensity-based registration methods basically register a pair of images by maximizing the correlation [7, 13] or simply by using the intensity information inherent in the images [8-10]. On the other hand, feature-based registration methods match common features including geometric and contour properties present in the image pair. Intensity-based methods are however less complex than the feature-based methods and hence can be employed effectively in automatic image registration algorithms. Registration algorithms can also be global or local based on the details attempted to be registered. Global registration procedures tend to register the image as a whole whereas local procedures refer to registration of certain selected organs only.

Intensity-based registration algorithms make use of the voxel intensity information inherent in the images. Such methods involve the optimization of a similarity measure of all the geometrically corresponding voxel pairs in the images. The greatest advantage of the intensity-based methods is that they can be automated. Commonly used intensity-based registration algorithms include minimization of variance, maximization of correlation co-efficient and maximization of mutual information. The maximization of

mutual information has been demonstrated as a powerful criterion for automatic registration algorithms [9, 10].

Image segmentation is the process of separating certain regions of interest from the image background and from each other [15]. Segmentation algorithms make use of the intensity information inherent in the images to achieve the desired segmentation of a selected region of interest. Segmentation is usually achieved by sectioning out the region of interest completely from the image or by tracing the contour of the region, depending on the problem requirements. Earlier methods of segmentation involved region growing and linking or using the image histogram to segment the desired region. Other, relatively new methods involve using vectors and gradient to trace out the contours of a region [16-18]. Clustering based segmentation methods fall under the region growing category and are used widely in medical image segmentation problems because of their simplicity and effectiveness.

## 1.5 Organization of Chapters

The next chapter describes the data that were collected for the testing and its pre-processing. Chapter 3 explains in detail about the implementation and testing of the registration algorithm, initially. Later sections of this chapter describe some of the results that were obtained using the registration algorithm. Chapter 4 describes in detail about the segmentation algorithm implementation, its testing and results. The thesis work concludes with Chapter 5 where some discussions about the methodology developed are made and the future scope of the thesis research work is outlined.

# CHAPTER 2

# DATA ACQUISITION AND PRE-PROCESSING

## 2.1 Data Acquisition

The data used for the testing of the developed algorithm were axial images of the abdomen obtained using Magnetic Resonance Imaging and Computed Tomography imaging. Three dimensional image volumes with about three to five slices, encompassing the entire pancreas were used as input images to the algorithm. Data with individual slice thicknesses of 3mm, 5mm, 7mm and 9mm were used in different trials to test the algorithm. MR and CT images of the abdomen with and without contrast agents were used. The initial testing phase for intra-modality image registration and segmentation was done using about four different CT datasets and three different MR datasets. Later testing phases involving inter-modality (MR and CT) image registration and segmentation were done using five different MR and CT datasets. Each of these five datasets comprised of abdomen images of the same region for a particular patient as done by MRI and CT imaging. However, the individual slice thickness of the images obtained using the two different modalities were not the same. Also, all the images were scanned during two different sessions (for MR and CT respectively) with a significant interval of at least six months between each of the sessions.

MRI data was acquired using a 1.5 Tesla GE scanner. The images were T1 weighted and some images were also fat-suppressed. CT data was obtained using a spiral (or helical) CT scanner. For CT images with contrast, oral contrast agents were administered to the patient. The raw images thus obtained were in the popular DICOM

format with a resolution of 512 voxels by 512 voxels and were 256 bit grayscale images. Most the raw (or un-processed) MR images were corrupted with background noise and contrast variations in the image. Almost all of the raw CT images had the ring artifact inherent in them. These artifacts were eliminated from the test images by using certain pre-processing methods as explained in section 2.2 of this chapter. The data resolution was also reduced to half (256 x 256) prior to using them as inputs for testing the algorithm developed in the present work. This was done to increase the speed of the overall procedure.

## 2.2 Data Pre-processing

Different data pre-processing routines were developed in the present work to eliminate some of the most commonly occurring intensity artifacts in the raw MR and CT images. These pre-processing routines were implemented as functions in MATLAB (using image processing toolbox and statistical toolbox) and used on the data prior to them being given as inputs to the registration and segmentation algorithm. Numerous trials were run using the different pre-processing routines and it was found that such kind of pre-processing enhanced the accuracy of the developed algorithm as well as ensured clearly distinguishable features in the abdomen. The pre-processing functions thus developed are briefly explained below.

### 2.2.1 Intensity Adjustment

This routine corrected the non-uniform intensities along a particular organ in the abdomen. This was done by adjusting the intensity value of each voxel to linearly stretch

the image histogram and span the entire grayscale range. This pre-processing routine was developed as a function in MATLAB. (Refer Appendix A)

In the case of CT images, the image contrast was improved by this pre-processing routine and the resultant image showed various abdominal organs with clearly defined borders as opposed to the raw CT image. In other words, image volumes with uniform illumination were obtained thus increasing the amount of 'information' that could be inferred from the images. The MR images obtained by using a contrast agent had non-uniform intensity thus making some parts of the abdomen look very bright (or white) and certain parts very dark. This pre-processing routine reduced this non-uniform illumination and in addition also removed background noise which occurred in certain cases. Some of the results obtained on preprocessing CT and MR images are shown in the Figures 2.1 and 2.2 respectively.

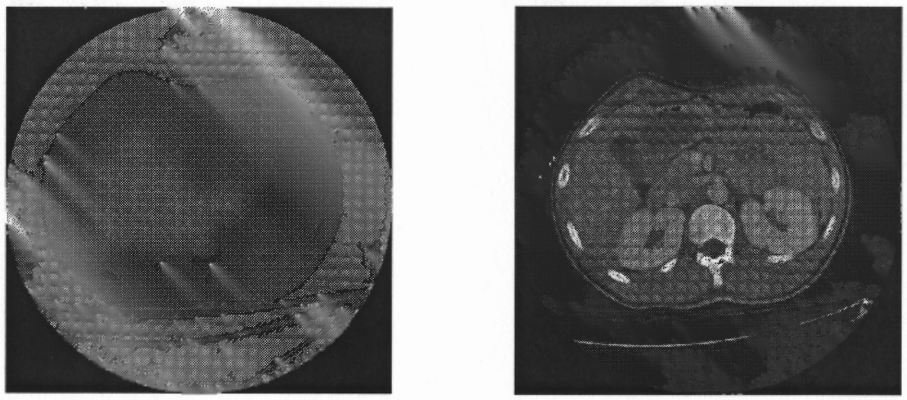

**(a)** **(b)**

**Figure 2.1** (a) A raw axial CT slice of the abdomen, before intensity adjustment, (b) The same CT slice after pre-processing. Intra-abdominal organs are shown much clearly in Figure 2.1b.

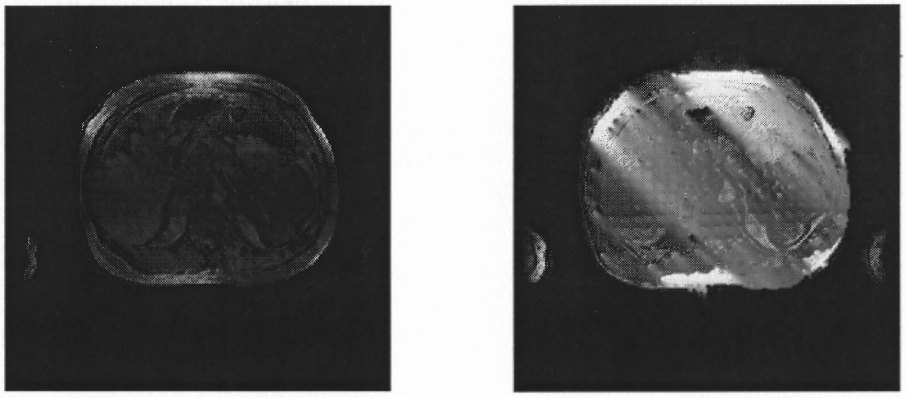

(a) (b)

**Figure 2.2** (a) Raw axial MR image of the abdomen as obtained from the scanner, (b) The same MR image after intensity adjustment. Intensity distribution is comparatively more uniform in Figure 2.2b.

### 2.2.2 Image Slices Stacking

In this procedure, individual slices of an image volume were stacked about the centroid of the image volume and with respect to the preceding slice. More clearly, the entire image volume was centered about the spatial grid representing the image volume. Then a 2D image registration technique was employed where initially the first slice was used as the 'reference' image and the next slice (above it) was assumed as the 'target' image and then aligned respectively. Then this registered slice became the reference image for the next (i.e., the third) slice. After registration this third slice became the reference for the fourth slice and so on.

This helped to compensate for uneven alignment of slices in a large volume. Such misalignment in slices can also be assumed as a shearing artifact along the X and Y directions (that occurs due to patient breathing in the scanner) and the slice stacking routine can be assumed as a crude shear pre-correction procedure.

Simulation results showed that such pre-processing procedure helped to improve the overall registration process. These results are outlined in the next chapter.

# CHAPTER 3

# IMAGE REGISTRATION

## 3.1 Introduction

Image registration is the process of mapping two images spatially such that corresponding structures overlap [19]. A geometrical transformation estimates a "transformation map" that aligns a 'target image' with a 'reference image' on a voxel-by-voxel basis, in the process of registration [20]. Medical image registration finds its use in aligning and comparing two images of a particular region of the human body, in both intra-modality (e.g.: MRI scans done on different days) and inter-modality imaging (e.g.: MR and CT) [21]. Image registration is broadly divided into manual, semi-automatic and automatic registration methods.

Manual registration methods are interactive methods that require a trained user to perform the registration using known anatomical landmarks. The user is assumed to have familiarity with the anatomical structures and mathematical skills to identify and decide about the kind of transformation required to facilitate registration of the images [5]. The transformation is then used based on the annotated regions drawn by the expert user to register the two or more images. A computer based numerical interpretation of the registration between the images is used as a guiding factor by the user to carry out the process. These methods are labor intensive as each of the objects (or organs) from each image slice have to be labeled individually by an expert user prior to any kind of registration. Such methods, apart from being time-consuming, also suffer from user subjectivity and hence are not very effective.

In semi-automated registration methods, the user interaction is limited to selecting certain image features or parameters to be used in registration. The user might also have to specify the algorithm to be used, the initial conditions and the convergence and stopping criteria [5]. For example, contours of an object or organs may be used as a parameter and correlation coefficients between the contours of the two images may be used as the goodness of fit criteria to determine the alignment between the images. Such user-interaction can increase the efficiency of the registration process in certain cases.

Automatic methods of image registration require minimal form of user interaction during the registration process. The user needs to provide only certain basic criteria about the image acquisition as input to the registration algorithm [6]. Automated registration methods usually rely on intrinsic properties such as image contours (when a contour definition criterion has been pre-defined) and image intensity. Examples of such automated methods are geometrical landmark-based registration and voxel property-based registration. Even though automatic registration methods are widely preferred, there always exists a trade-off between minimal interaction and speed, accuracy, robustness of the automatic registration algorithm.

Signal intensity based correlation analysis is a typical example of an automatic registration method. As per this method, two identical images, one of which is shifted prior to registration, will have the highest possible correlation (= 1) once they have been registered correctly. Thus, one can use this criterion to register images in an automated fashion. However, there are certain assumptions made by this method. First, it assumes that the two or more images to be registered have the same image characteristics (e.g., they are both CT images of similar intensities containing the same organs). Secondly, the

motion is assumed to have caused all the features (organs or tissue types) to be shifted in a similar fashion. Third, the noise properties between the two images are assumed to be similar.

The above mentioned assumptions are not satisfied in a number of cases, particularly when images are obtained using different modalities. Further, even while using the same modality, if there is a growing tumor in the image whose size is changing, then intensity based correlation analysis cannot be used. Hence, intensity based correlation analysis is seldom used in image registration even though it is computationally efficient

In recent years, a novel registration algorithm based on mutual-information has been developed by Viola *et al.* [9] and Collignon *et al.* [22]. Mutual information (MI) is a basic concept from information theory and measures the entropy (amount of information) that one image contains about the other, statistically. Image registration by using mutual information involves the maximization of mutual information (MMI) criterion [10]. The MMI registration criterion depends only on the relative occurrence of the voxels in the images to be registered and it makes no assumptions regarding the image characteristics [8-10]. As a result, this criterion is preferred over the intensity based correlation analysis and is currently being used to automatically register both intra-modality as well as inter-modality image volumes.

The next important criterion to be considered in the implementation of a registration algorithm is the geometric transformation that will map or align one image to another. The commonly used geometrical transformations in the registration problem are rigid, affine, projective and elastic (or curved) transformations [6, 19]. In rigid

transformations (for example in the brain), only translations and rotations are allowed. Affine transformation maps parallel lines onto parallel lines. Projective transformation maps lines onto lines while elastic transformation maps lines onto curves [6, 19]. The geometric transformation that an image registration algorithm uses is directly related to the type of distortions that might occur in the images during the imaging procedure.

In this thesis work, mutual information based registration algorithm was implemented to register abdominal images obtained from subjects, using both CT and MRI. The algorithm was implemented to take into account a number of displacement parameters. In the case of abdominal images, the major distortions occur due to the effects of patient motion and patient breathing in the scanner. These were modeled as rigid transformations and affine transformations respectively. Thus, the optimization problem this thesis was the maximization of mutual information. Although, numerous methods exist [25], in this thesis, a *down-hill simplex* based optimization routine was chosen. This method, apart from being simple, is also a quick and effective mathematical technique that can be used for intensity-based image registration and hence was employed in the registration algorithm developed.

## 3.2 Theory

### 3.2.1 Mutual Information

The Mutual Information (denoted as I) between two images A and B can be represented as:

$$I(A,B) = H(B) - H(B \mid A) \qquad 3.1$$

where, *H(B)* denotes the entropy of image B or the amount of uncertainty about image B and *H(B|A)* denotes the conditional entropy or the amount of uncertainty about B when A is known[8].

A decrease in the overlap between two images (more misregistration) would result in reduced statistical power of the probability distribution estimation which measures the entropy. Recent studies of Studholme *et al* [24] has shown that a *normalized mutual information* measure can be used alternatively as it is less sensitive to changes in overlap [8]. The normalized mutual information between two images A and B can be represented as below:

$$NMI(A,B) = \frac{H(A) + H(B)}{H(A,B)} \qquad 3.2$$

where *H(A)* and *H(B)* are called the marginal entropies of images A and B respectively and *H(A,B)* denotes the joint entropy.

When the image intensity or the grey level values are used as a measure of information, the entropy for an image can be computed using the probability distribution of its grey values. This probability distribution can be estimated from the histogram of the image. An image having a histogram with a sharp peak (all voxels of a single intensity) would thus have a low entropy value as it contains very little information. An image having a dispersed histogram that has many different intensity values would contain a lot of information about the image, from an information theoretic sense. Such an image would yield a high value of entropy. For two images, the MI is computed from the joint probability of the image intensities. Joint and marginal distributions are estimated from the joint and marginal histograms of the overlapping parts of the image respectively. When two images are perfectly aligned, there is more overlap and the

resulting joint histogram has a characteristic sharp peak. This results in a low joint entropy value which in turn results in a high MI value [8, 10]. Joint histogram thus provides a measure of entropy between the images and the MI can therefore be computed by constructing a joint histogram of the images to be registered [10].

### 3.2.2 The Down-hill Simplex Optimization Routine

The mutual information measure was maximized by using the down-hill simplex optimization routine as suggested by Nelder and Mead [23]. This method evaluates a function directly and does not require function derivatives to be computed. Hence, the down-hill simplex method gives an approximate result only but is computationally less expensive and faster compared to other traditionally used methods [25].

The method starts by defining a simplex based on the number of independent variables of the function to be minimized. A simplex is a geometrical Figure in 'N' dimensions consisting of N+1 vertices (In three dimensions, a simplex is a Figure with four vertices i.e., a tetrahedron). An initial starting guess for the vertices of the simplex is required by this method. Once such a simplex is constructed, the method uses three basic operations viz. reflection, expansion and contraction to find the local minimum of the function. Each of these operations tends to reduce the size of the simplex structure to converge around the 'minimum' point. The convergence criteria and the step size for each iteration that reduces the simplex size are specified by means of a tolerance function. The method begins from the highest point (or peak of a hill) in the vertex of the simplex and gradually works its way down to the minimum point – called the valley of a hill. As this minimization technique goes 'down the hill' from the peak to the valley

point, it is termed as down-hill simplex method [23, 25]. Figure 3.1 shown below illustrates the concept of a simplex and its optimization.

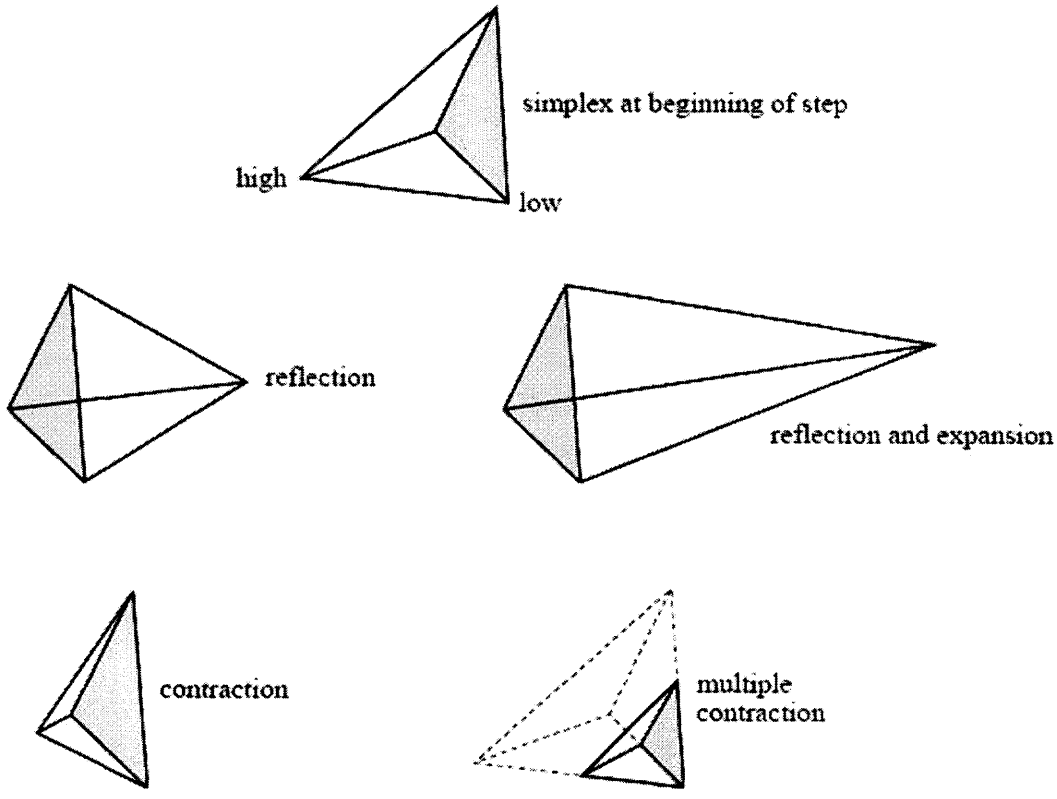


**Figure 3.1** Different methods used in the optimization of a 3D simplex (a tetrahedron) to yield the minimum value. [25]

### 3.3 Implementation and Testing

The normalized mutual information measure with the down-hill simplex optimization routine was used in the registration algorithm. To register a pair of image volumes, a reference image volume (or a source image volume) and a target image volume were defined respectively. For MMI based registration, the registration problem is defined as finding a co-ordinate transformation that transforms the target image coordinates into reference image such that the mutual information is maximized [9, 10]. In the case of

abdominal image volume registration implemented in this thesis, rigid body and affine transformations were applied. The registration thus involved optimization of six parameters – three translations, one rotation, two affine scaling and one affine shearing.

The image registration algorithm was implemented in three basic sub-registration steps. In the first step, the algorithm aligned the images to compensate for the *linear shift* or *translational shift* between the target and reference images along the X, Y and Z directions of the spatial grid representing the images. In step two, registration was performed on the linear-shift corrected target image to compensate for *affine scaling and shearing* along the horizontal and vertical directions (the X and Y axes). The final step or step three performed a sub-registration routine on the target image as obtained from step two, to compensate for *angular shift* or *rotational shift* about the Z axis of the spatial grid representing the image. The linear and rotational shifts were assumed to occur in the images due to patient motion in the scanner. The affine scaling and shearing were assumed to be the effect of (uneven) patient breathing during the imaging procedure.

The initial guess values for the down-hill simplex optimization algorithm were estimated using the reference and target images automatically instead of the user having to specify them. In the case of the linear-shift sub-registration procedure this was done by initially computing the centroid of both the images. Then, by calculating the difference in the centroid of the target image with that of the reference image, the approximate linear shift of the target image was determined. The first sub-registration procedure then aligned both images in the spatial grid to compensate for the difference in centroid values. This was done by computing the mutual information between reference and target images and optimization of the mutual information value in steps or iterations till the maximum value

was obtained. The parameters of the function for which maximum mutual information was obtained yielded the values by which the target image had to be shifted to be best aligned with the reference image.

Image alignment using an affine shearing and scaling transformation was also done in a similar manner as the process described above. In this case an affine matrix, as shown below, describing the shearing and scaling in the image was defined.

$$A = \begin{bmatrix} s_x & sh_{xy} & 0 \\ 0 & s_y & 0 \\ 0 & 0 & 1 \end{bmatrix} \qquad 3.3$$

$s_x$ and $s_y$ denote the values of scaling along the X and Y directions respectively and $sh_{xy}$ denotes the shearing along the X-Y plane.

The values of the matrix, corresponding to the best registration, were obtained by maximizing the mutual information between the reference image and the aligned target image, as obtained in the previous step. The initial values for shear and scaling in the affine matrix were assumed as '1' (i.e., $s_x = s_y = sh_{xy} = 1$) and the mutual information was computed. The optimization routine then maximized the mutual information value iteratively and yielded the affine matrix corresponding to the best registration between the images.

Finally, the rotational shift correction was also done. To compute the best initial guess value, the target image was aligned with the reference image for unit degree increments of a range of values and the mutual information was computed for each alignment. This was done as follows: the target image was shifted from -10 degrees to +10 degrees (in 1 degree increments) with respect to the center of the reference image (i.e., about the Z axis) and for each unit shift the mutual information was computed. The

best possible match thus yielded the maximum mutual information value. The guess value was simply chosen as the point where this maximum mutual information value occurred. This method however limited the accuracy of the angular shift correction routine to ±10 degrees. Numerous trials on test datasets showed that the assumption of a rotational shift being more than ±5 degrees seemed unrealistic particularly for the set objective in the present work.

Once the guess value was determined, the rotational shift sub-registration was done by optimizing the mutual information between the reference image and the target image as obtained after affine shift alignment. Thus, the overall registration was achieved in three steps which corrected the linear shifting along X, Y and Z axes, rotational shifting about the Z axis and the affine shape changes along the X-Y plane.

The three step registration procedure was implemented in MATLAB. Independent functions for determining the guess values at each stage were also developed.

### 3.3.1 Inter-modality Registration

MR and CT images of the abdomen imaged for the same patient at different points of time were registered using the basic registration algorithm developed. Such inter-modality registration becomes imperative to register certain anatomically important sections in the abdomen images so that a comprehensive analysis of a pathological condition can be done using the images from both the modalities. In the present case, MR images which had clearly distinguishable features comparatively were used as reference images and the CT images were assumed to be the target images and thus registered with respect to the MR image volumes.

The algorithm implemented for this purpose was robust in the sense that it could be incorporated even if the CT and MR images of the abdomen did not encompass exactly the same regions. For example the MR image volume could have started from the chest region all the way to the abdomen region and the CT could have covered only the abdomen region. In such cases, the registration problem also includes initially identifying and selecting the similar regions and then registering them. The registration algorithm for inter-modality registration was developed so as to automatically identify and register slices containing only the same anatomical features.

The initial step in the algorithm converted the individual slices in the MR and CT volumes to a uniform thickness of 1mm each. The median (center) three slices were then selected from the target volume. The best match for these three slices in the entire reference image volume was then determined by performing registration at reduced resolution. This was done by reducing the resolution of the three median slices from the target image volume and the reference image volume to half the original resolution. Then registration was done between the first three slices of reference image volume and the three median slices selected from the target image and the mutual information value of the registered images was computed. Next the median slices of the target were registered with the next three successive slices of the reference in hierarchical order (i.e., slices 2, 3 and 4) and the MI value was computed. The next registration was done between the median slices and slices 3, 4 and 5 of the reference volume and the MI value was computed.

This process was continued till the three median slices were 'compared' or registered with each set of three successive slices in the reference image. Based on the registration which yielded the maximum mutual information value, the best match in the reference image was found. This was the portion of the reference image which best matched with the center of the target image and using this valuable detail, regions representing similar anatomical structures in the reference and target image were obtained. The final step was the registration (at actual resolution) of the two similar anatomical regions represented in the reference (CT) and target (MR) image volumes.

The inter-modality image registration procedure was tested using five different CT and MR images of the abdomen, where each of the CT and MR combination represented the same regions in the abdomen of a patient. In four of these five test datasets the MR volume had a different individual slice thickness compared to the CT volume individual slice thickness. One trial was run with MR and CT volumes having the same individual slice thickness. In each of these trials the similar anatomical regions that had to be registered was a subset of the image volume. The registration algorithm initially identified the corresponding subsets of anatomically similar regions in both the reference and target image volumes and then registered the regions successfully.

### 3.3.2 Intra-modality Registration

In some practical cases, two image volumes of the same region imaged using the same modality but at different points of time need to be registered for analytical purposes. A typical example of a situation where intra-modality registration becomes necessary is during post-operation or post-treatment analysis. In the present work, the registration

algorithm described above was used to register similar slices from two different image volumes imaged by the same modality, where one image volume was simulated as the target image. Test simulations to register different set of consecutive slices from the same image volume were also run to evaluate the efficiency and robustness of the algorithm developed.

Abdominal images of different subjects were obtained using the standard imaging protocols. The different effects of patient motion were then simulated on these images and thus the reference and target images for registration were obtained. In most of these trials, only those slices in the image volume that encompassed the entire pancreatic region were considered while in some of the trials the entire image volume was considered. MRI and CT abdominal images from 7 patients totally were used in this study. The number of slices in each dataset varied from 3 to 9.

### 3.3.3 Simulation of the Test Images

The effects of patient motion were simulated by linear and rotational shifts that were assumed to shift the target image volume by ±10 voxel units and ±10 degrees respectively, with respect to the center of the reference image. Effects on the abdominal image due to patient breathing were simulated by an affine transformation that sheared, stretched and compressed the image dimensions in both X and Y directions. The image volume was assumed to stretch and compress by a maximum of 20% of its original size in the horizontal as well as vertical directions, due to patient breathing. A minimal amount of shearing resulting in a 5% distortion along the X-Y plane was also simulated by the affine transformation. Motion induced signal changes were simulated using 100 different possible combinations on a single dataset, and thus 100 trials were run using a

single test dataset. Results obtained for each dataset were analyzed statistically which facilitated the quantitative performance analysis of the developed registration algorithm.

The performance of the registration algorithm was evaluated based on the simulated distortion values. The differences between the actual and the estimated registration parameters were found after the reference image and the simulated target images were registered. The misregistration was thus quantified based on the difference values (or the error values).

For inter-modality registration, the performance of the algorithm was evaluated by subtracting the reference and target images before and after registration. This basically showed the displacement between the images before and after the registration process, visually. Further evaluation of the inter-modality registration was done based on the number of misregistered pixels before and after registration [26].

## 3.4 Results

### 3.4.1 Intra-modality Registration

Table 3.1 shows the average error values (mean± standard deviation) obtained after performing 100 trials of the registration procedure on four different CT datasets. Table 3.2 shows the same results obtained by using three different MR datasets. The error values were computed as the difference between the actual registration parameters (that were used to simulate a target image) and the registration parameters estimated by the algorithm (when aligning the simulated target image with the reference image). The overall average error rate with which the algorithm could register the images in the four CT volumes was 0.115±0.19, 0.106±0.25, 0.116±0.23, 0.132±0.28 respectively. The

overall average error rate with which the algorithm could register the images when the three MR volumes were used was 0.164±0.26, 0.145±0.29, 0.162±0.34 respectively.

**Table 3.1** Error Values for Intra-modality Registration of CT Abdomen Volumes

| | Dataset1 | Dataset2 | Dataset3 | Dataset4 |
|---|---|---|---|---|
| Linear-shift along X axis (voxel units) | 0.13± 0.342 | 0.11± 0.501 | 0.10± 0.485 | 0.11± 0.489 |
| Linear-shift along Y axis (voxel units) | 0.15± 0.340 | 0.09± 0.480 | 0.12± 0.324 | 0.10± 0.421 |
| Linear-shift along Z axis (voxel units) | 0.02± 0.141 | 0.06± 0.239 | 0.02± 0.141 | 0.09± 0.297 |
| Rotational-shift about Z axis (degrees) | 0.38± 0.310 | 0.37± 0.221 | 0.45± 0.397 | 0.48± 0.456 |
| Horizontal affine correction (x100 %) | 0.005± 0.032 | 0.005± 0.008 | 0.005± 0.005 | 0.007± 0.005 |
| Vertical affine correction (x100 %) | 0.004± 0.030 | 0.002± 0.029 | 0.003± 0.028 | 0.003± 0.023 |

**Table 3.2** Error Values for Intra-modality Registration of MR Abdomen Volumes

| | Dataset1 | Dataset2 | Dataset3 |
|---|---|---|---|
| Linear-shift along X axis (Voxel units) | 0.18± 0.392 | 0.17± 0.410 | 0.11± 0.492 |
| Linear-shift along Y axis (Voxel units) | 0.06± 0.571 | 0.08± 0.550 | 0.12± 0.334 |
| Linear-shift along Z axis (Voxel units) | 0.11± 0.311 | 0.11± 0.311 | 0.09± 0.376 |
| Rotational-shift about Z axis (degrees) | 0.62± 0.282 | 0.48± 0.501 | 0.61± 0.837 |
| Horizontal affine correction (x100%) | 0.013± 0.010 | 0.015± 0.016 | 0.016± 0.019 |
| Vertical affine correction (x100%) | 0.003± 0.021 | 0.02± 0.011 | 0.027± 0.006 |

Figures 3.2 and 3.3 show the results of registering the simulated target images with the reference images, for CT and MR imaging respectively. The misalignment between the reference and target images was indicated by subtracting both the images as illustrated in Figures 3.2c, 3.3c and Figures 3.2e, 3.3e respectively.

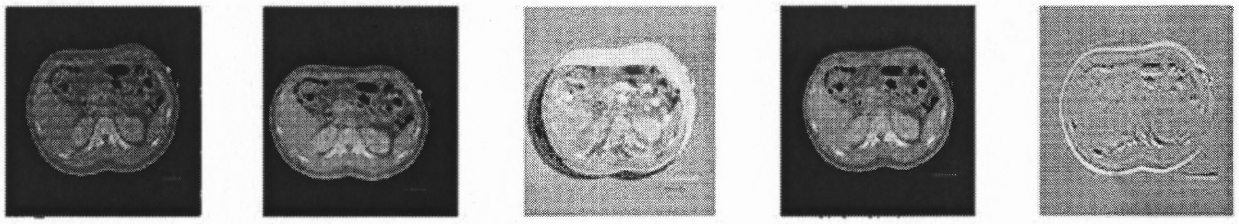

(a) (b) (c) (d) (e)

**Figure 3.2** (a) Reference CT image, (b) Simulated 'target' CT image, (c) Misregistration in reference and target images before registration, as obtained by image subtraction, (d) Target image after registration, (e) Misregistration in reference and target images after registration, as obtained by image subtraction.

(a) (b) (c) (d) (e)

**Figure 3.3** (a) Reference MR image, (b) Simulated 'target' MR image, (c) Misregistration in reference and target images before registration, as obtained by image subtraction, (d) Target image after registration, (e) Misregistration in reference and target images after registration, as obtained by image subtraction.

Figure 3.4a shows the joint histogram for two same CT images (i.e., images with similar intensity distribution). As explained earlier in the chapter, when identical images overlap their intensity distributions are perfectly aligned. Hence the joint histogram has a sharp diagonal line as shown in Figure 3.4a.

When the identical images do not overlap, the combined image would have a dispersed joint histogram. This is because of the repetition of various structures of the identical images in the combined image (as they do not overlap). This is illustrated in Figure 3.4b which shows the joint histogram of the identical CT slices before registration respectively.

When two images of the same scene do overlap, there is alignment of the corresponding structures (i.e., no repetition of similar structures in the combined image). In such a case, the joint histogram would appear less dispersed and more clustered compared to when the images were misaligned. Figure 3.4c shows the joint histogram of the aligned CT slices after the registration process. It can be seen that there is more uniform clusters in this image compared to Figure 3.4b. However, the joint histogram may not be a diagonal as in the ideal case because of registration and interpolation errors that tend to affect the intensities of the similar structures in each of the images [10].

The normalized mutual information (NMI) values between the images before registration and after registration were 1.1215 and 1.5798 respectively.

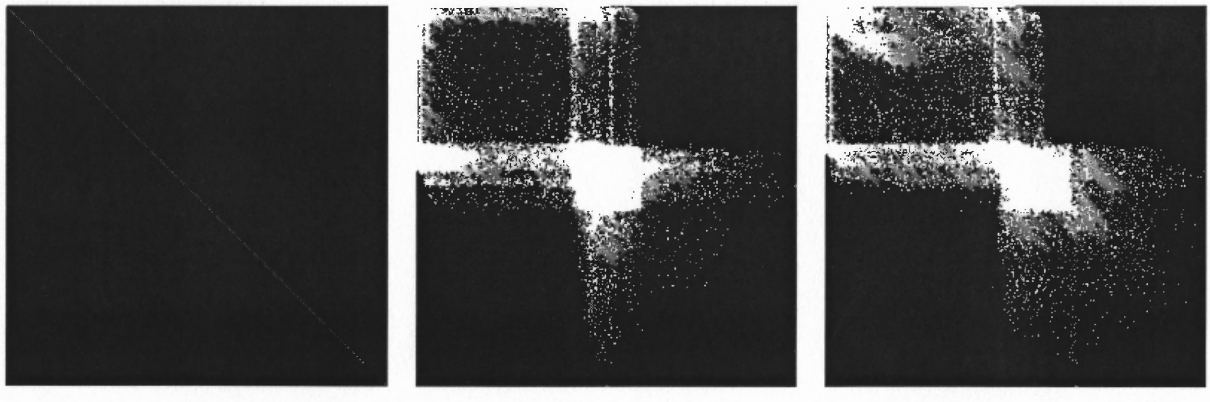

**(a)** **(b)** **(c)**

**Figure 3.4** 2D joint histograms for (a) two identical images, (b) the unregistered CT volumes (NMI = 1.1215) and (c) registered CT volumes (NMI = 1.5798).

### 3.4.2 Inter-modality Registration

Figure 3.5 shows the number of misregistered pixels in the CT-MR datasets containing the same regions, before and after registration. Registration of the images reduced the percentage of misalignment as evident from the Figure. However, as the data corresponded to the same patient (but different modality) and was aligned to a certain extent, there was a minor difference in the percentage of misregistered pixels before and after registration as seen in the Figure.

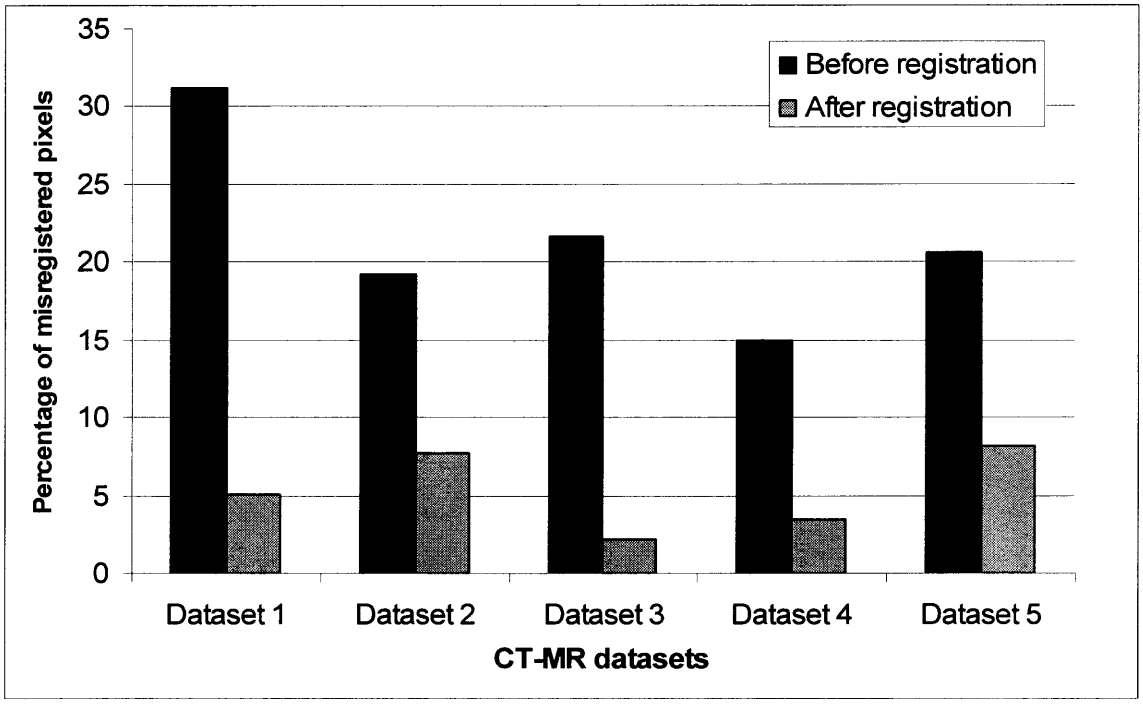


**Figure 3.5** Plot of misregistered pixels before and after registration of same patient CT-MR dataset.

Figures 3.6a to 3.6d shown below displays the registration results for one of the patients' CT and MR dataset. The target image volume was a CT volume image of the abdomen having twenty slices of 2.5 mm thickness each. The reference image was an MR image volume of the abdomen with seven slices and an individual slice thickness of

8 mm. The four slices in the Figure 3.6a and 3.6b correspond to the slices of MR and CT representing regions of similar anatomical regions respectively. The four slices in Figure 3.6c show the misregistration between the images before registration, by image subtraction. The four images in Figure 3.6d show the difference between the images after they are registered. The normalized mutual information (NMI) value of the volumes before registration was 1.0855 and after registration was 1.2515. The reduction in misalignment between the images is evident from Figure 3.6d and from the normalized mutual information values before and after registration. Intensity stretching technique was employed while displaying the difference between the images, in order to show the misalignment more clearly.

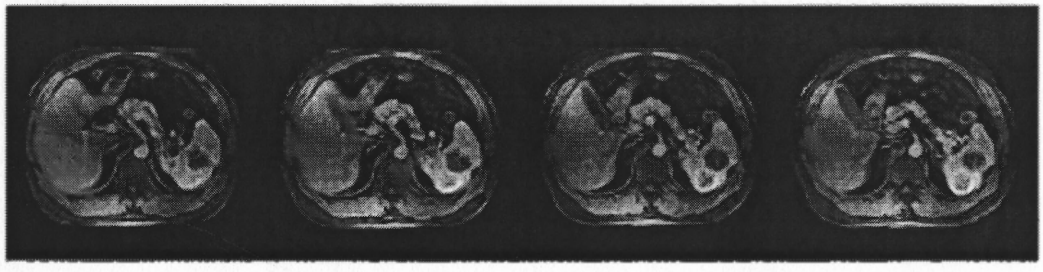

**Figure 3.6a** Four slices of the MR image volume encompassing the pancreatic region.

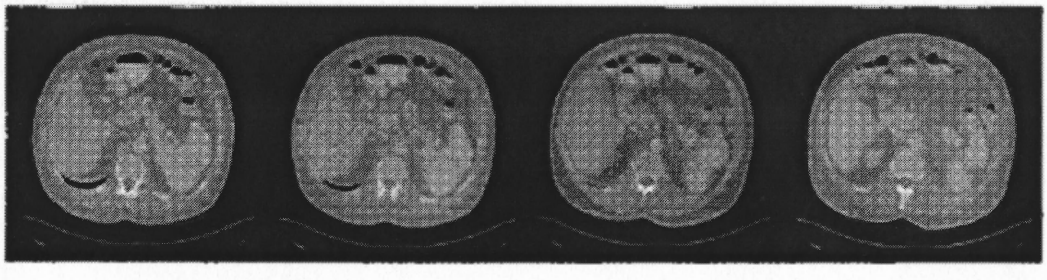

**Figure 3.6b** Four slices of the CT image volume encompassing the pancreatic region.

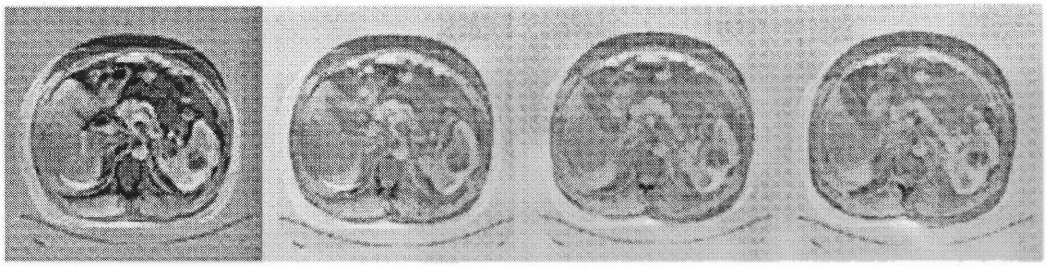

**Figure 3.6c** Misregistration between the four slices before registration, shown by image subtraction. (NMI value = 1.0855)

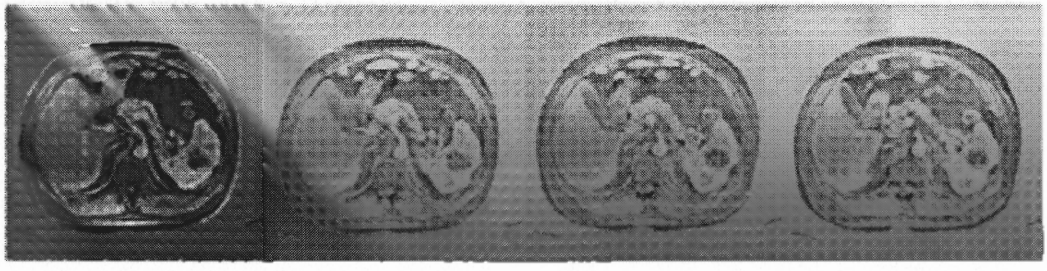

**Figure 3.6d** Misregistration between the four slices after registration, shown by image subtraction. (NMI value of = 1.2515)

Figure 3.7 shows the joint histogram comparison of the CT-MR registration procedure, before and after registration respectively. As seen from Figure 3.6a, the MRI slices tend to have distinct intensity values for different intra-abdominal regions. The CT slices (Figure 3.6b) however do show all the regions in the abdomen but individual regions do not have much intensity difference as compared to the MR images. Hence, even though both volumes represent the same regions / structures, their intensity distribution or histograms are different. Due to the different intensity distributions in the similar structures in both the images, the joint histogram of the registered images does not have a distinct diagonal line. Hence, registration in this case is validated by the dispersion of intensity values in the joint histogram.

Figure 3.7a shows the joint histogram before registration of the MR and CT slices. Due to misalignment in the corresponding structures, there is a pronounced dispersion of the intensity values. Figure 3.7b shows the joint histogram after the registration process. Here, the joint histogram has less dispersed and more compressed (or clustered) intensity values due to the successful overlap of similar regions (with different intensities).

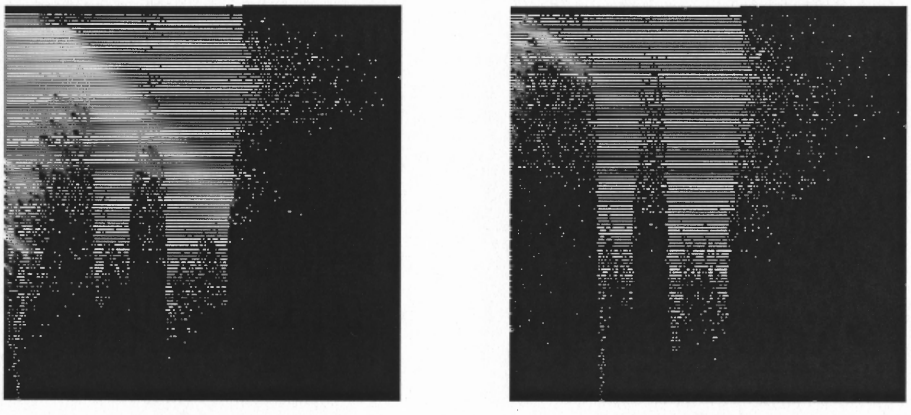

(a) (b)

**Figure 3.7** 2D joint histogram of the CT-MR dataset (a) before registration and (b) after registration.

# CHAPTER 4

# IMAGE SEGMENTATION

## 4.1 Introduction

Image segmentation is the process of separating regions of interest from an image. Once separated, specific information about the segmented region is typically inferred or compared with other regions. The medical image segmentation problem involves separating or segmenting regions pertaining to a particular organ or tissue type. These regions typically have homogenous intensity in the image [14]. Segmentation of medical images can help facilitate the study of anatomical structures from a region for diagnosis and treatment of a certain pathological condition in that region. A typical example is segmentation of the pancreas from the abdomen for the diagnosis and treatment of pancreatic cancer.

Image segmentation methods are specific to the requirements of the problem and hence a wide variety of segmentation algorithms exist in literature [14]. The segmentation algorithms can broadly be grouped as clustering-based methods [18-23], histogram-based methods [14], region-growing methods [14], contour-based methods [15, 16] and model-based segmentation methods [17]. The segmentation procedure employed using one of these algorithms can either be automatic or interactive (semi-automatic). In the case of automatic segmentation methods, an 'atlas' image is supplied to the algorithm. The algorithm then identifies the region that best matches with the atlas image provided and segments the region accordingly. Semi-automatic methods require

user inputs that specify the seed points in the regions of interest or trace out contours of the regions to be segmented.

Clustering-based methods segment the regions of interest by clustering or grouping the pixels (or voxels in the case of a 3D image) of homogenous intensity values. The procedure does not use any image context-related details such as the shape and relative position but relies on the intensity values only [15]. This makes the segmentation by clustering a relatively simpler and a faster process. Also, this method can be employed effectively for segmentation in all kinds of different medical images, as it depends only on the pixel (or voxel) intensity values. Due to these characteristics of the clustering-based segmentation methods, an interactive (semi-automatic) segmentation procedure based on the clustering algorithm was developed in this thesis for segmenting the pancreas.

A digital, 2D image is represented by individual picture elements or pixels, which describe the brightness (or resolution) of the image. In general, information about any digital image can be described by primary or first-order features i.e., pixel value (brightness) and spatial location of the pixel, and by certain higher order features that describe the relation of each pixel with its neighbors. These features can collectively be represented by an 'n' dimensional vector called the feature space. The segmentation problem by clustering is thus to partition the feature space into different mutually exclusive and collectively exhaustive regions [19].

In the methodology used in this thesis work, the feature space was assumed as the vector that describes only the first-order features of the images i.e., the image intensity. Thus, the matrix or the grid of pixels (voxels in the case of a 3D image) was initially

converted into a 1 dimensional vector representing the image. The data values in this vector were grouped or clustered iteratively by the k-means clustering algorithm [23]. The clustered vector was again converted back to a grid of pixels (or voxels) now representing the clustered image, where each cluster represented a homogenous region of the original image. Finally, using morphological operations, a contour was drawn around the region of interest, based on its clustering, thus achieving segmentation.

## 4.2 Methods

Clustering is the unsupervised process of grouping almost similar data based on certain criteria [30]. Numerous clustering procedures exist in literature for data classification. The initial phase in any clustering process is feature selection / extraction which involves identifying the seed points or the centroid points to initiate the clustering process. The next phase in the clustering procedure is determination of the proximity of individual data in each of the clustered patterns by a suitable distance measure. A variety of such distance measures exist and are used generally based on the definition and requirement of the clustering problem. Ultimately, based on the similarity of data within each pattern the clustering process is accomplished.

The clustering algorithms are broadly classified as *Hierarchical clustering* and *Partitional clustering* procedures [30]. Hierarchical clustering methods result in a nested series of partitions based on a similarity criterion for splitting or merging clusters [30]. However, such methods are computationally cumbersome. Partitional clustering methods attempt to identify a partition by optimizing a clustering criterion function that can be defined either locally or globally pertaining to the data to be clustered [30]. Partitional

clustering methods work effectively when the amount of data to be clustered is very large. However these methods require the number of desired output clusters to be necessarily specified. Majority of the clustering procedures used in image segmentation fall under this category. The k-means algorithm is one such partitional clustering algorithm which is widely used in image segmentation. The basic details about the k-means algorithm and its implementation in the present thesis for segmentation of pancreas from the abdomen images are explained later in this section.

Once the image was clustered into various regions, segmentation was achieved by automatically tracing the contour of the region of interest. In the present thesis, the cluster corresponding to the pancreatic region was selected and a series of mathematical morphological techniques were then employed to trace the contour of this pancreatic region. The traced contour was then overlaid on the original image to show the pancreas, thus segmenting it from the rest of the abdominal regions.

**The k-means Clustering Algorithm**

This algorithm was first proposed by MacQueen [23] in the year 1967. The k-means method is a statistical clustering procedure used to partition data into 'k' different groups or clusters, where 'k' is a positive integer. Each cluster is formed by minimizing the sum of squares of distances between individual data and the corresponding cluster centroid [31]. The Euclidean distance is the most commonly used distance measure to compute the variation of data within a cluster [19]. In the present thesis, the most basic k-means algorithm based on the squared Euclidean distance measure was implemented to facilitate image segmentation because of its simplicity and fast computing power.

The k-means clustering algorithm involves three basic steps:

1) Determination of individual cluster centroids (or seed points).

2) Computation of the distance of each data point from the respective cluster centroid.

3) Grouping data into respective clusters based on the *minimum* distance.

Initially, the 'k' cluster centroids are chosen either randomly or by a statistical process (eg: mean of a subset of data) to begin the data clustering. The numbers of cluster centroids thus chosen represent the desired number of clusters. Each of the data samples are then assigned to the respective cluster based on the minimum distance of the sample from the cluster centroid, which is the basic clustering or grouping process. Once these initial clusters are created, each cluster centroid is updated using all the data samples in that respective cluster. This step minimizes the distance between the samples and the centroid point in each individual cluster. The clustering process is repeated using the newly computed centroid values. Once the new clusters are obtained, the distance minimization by re-computing the centroid point is done again and the clustering process is repeated. This iterative process is continued till a termination criterion is reached (or till the algorithm has converged). The termination criterion or the convergence criterion denotes the point where no members of a cluster can change on further clustering.

The k-means clustering algorithm can be more clearly illustrated by the flowchart shown in Figure 4.1:

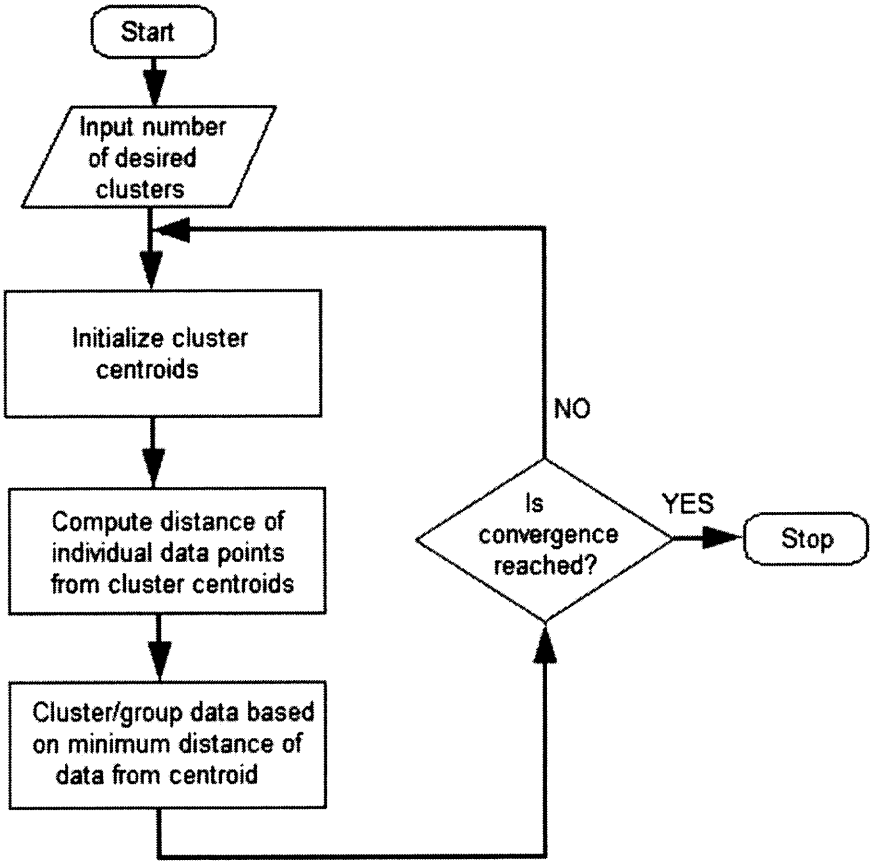


**Figure 4.1** The k-means clustering algorithm flowchart.

### 4.3 Implementation

The segmentation procedure consisted of a set of functions developed using MATLAB, specifically for the segmentation of pancreas from abdominal images. These custom-defined functions served as processing tools to cluster the image initially and then trace out the contour of the pancreas. The functions were developed for both 2D and 3D abdominal images obtained from MRI and CT imaging modalities. This segmentation

procedure could also be used for simple clustering-based segmentation of any 2D and 3D images in general.

There were six basic functions in the segmentation procedure to pre-process, cluster, segment and display the segmented sections. The flow diagram shown in the Figure 4.2 illustrates the sequence of steps implemented in the segmentation procedure to achieve the desired image segmentation.

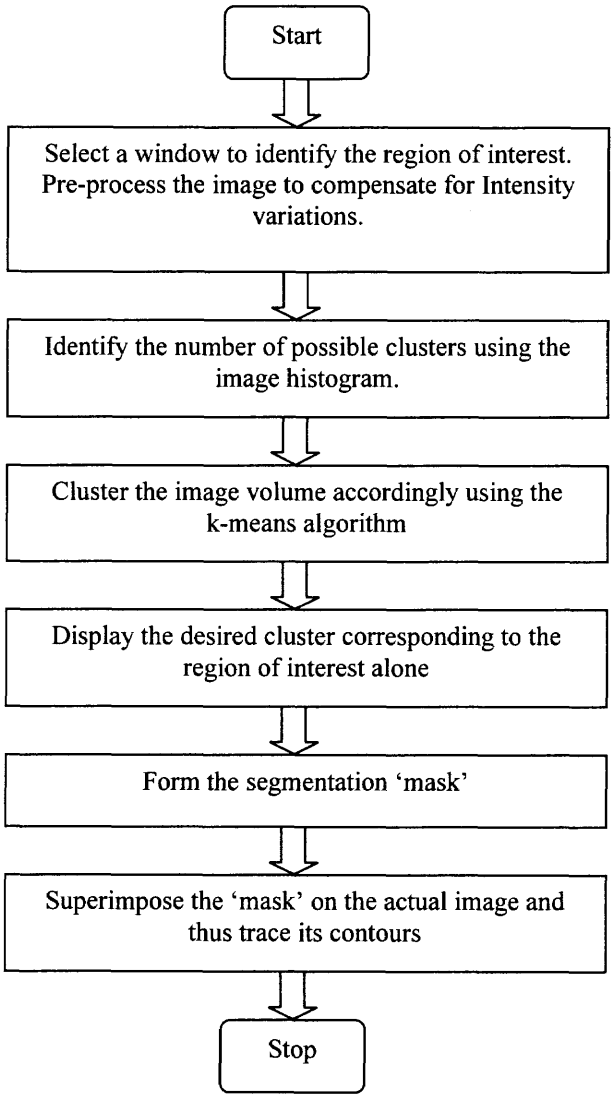


**Figure 4.2** Flow diagram showing the sequence of steps used for image segmentation.

The initial step of the procedure allowed the selection of a particular region of interest to be segmented, using a windowing technique. Once the region of interest was selected, a histogram equalization step was also performed to improve the image contrast. This basically resulted in a more homogenous clustering and thus better segmentation.

A necessary input to the k-means clustering algorithm is the number of clusters or groups the input data has to be divided into. In the present work, this was determined based on the number of distinct unimodal distributions in the image histogram [15]. As different organs in the abdomen have different and almost distinct intensity values, they manifest themselves as unique unimodal distributions in the overall image histogram. The number of clusters possible for any given image is thus equal to the number of distinct unimodal distributions seen in the image histogram. This logic was implemented in the present thesis along with an image smoothing step using a Gaussian filter. Smoothing removes spatial noise and thus helps to show the unimodal distributions more clearly. The number of possible clusters in the sectioned region of interest was thus inferred interactively.

Based on the number of clusters decided, the 3D image was clustered using the k-means algorithm. Initial selection of the centroid points or seed points was done by performing a preliminary clustering phase on a random sub-sample of the vector representing the image. The clustering function developed here used the built-in routine for k-means clustering available in the MATLAB statistical toolbox.

The cluster representing the region of interest was then selected interactively, by looking at the clustered output image and specifying the desired cluster number. A binary mask was then created by performing an image dilation operation on the selected cluster

and subtracting the dilated image from the original image. The subtracted result hence contained only the image contours. This mask was superimposed on the actual image, therefore highlighting its contours. Segmentation was thus achieved by tracing the contour of the region of interest, by this binary mask. The segmented region of interest can also be completely sectioned out from the original image by making minor modifications in some of the functions developed. Such a kind of masking-based, contour tracing segmentation procedure was developed in the present thesis basically to highlight the abnormalities in the pancreas

All the functions that were developed for the segmentation procedure are listed in Appendix C.

### 4.4 Testing and Results

The performance of the segmentation procedure was evaluated by testing it on different datasets under different test conditions. Initially, the procedure was used to detect the contour of the pancreas in MR and CT abdomen volumes using different number of clusters. Gaussian white noise with zero mean and different values of variance was added to the pancreatic image volumes and the procedure was used to segment the pancreas from such noise-corrupted image volumes. In such cases however, a morphological closing operation was performed after the clustering stage to generate a smoother closed contour around the pancreas. Finally, a comparison of this method with manually traced contours (of the pancreas) was done without and with the presence of a similar gaussian noise.

Figure 4.3 shows the results of segmenting the pancreas from the MR abdominal volume. A representative slice of pancreas is shown in the Figure. The approximate area in the abdominal region containing the pancreas was chosen by the windowing technique, prior to the clustering process. The number of clusters in the image was chosen as two based on the image histogram of this selected region. Figure 4.3a shows the contour traced region in the actual image and Figure 4.3b shows an enlarged view of the selected pancreatic section after its contour was traced.

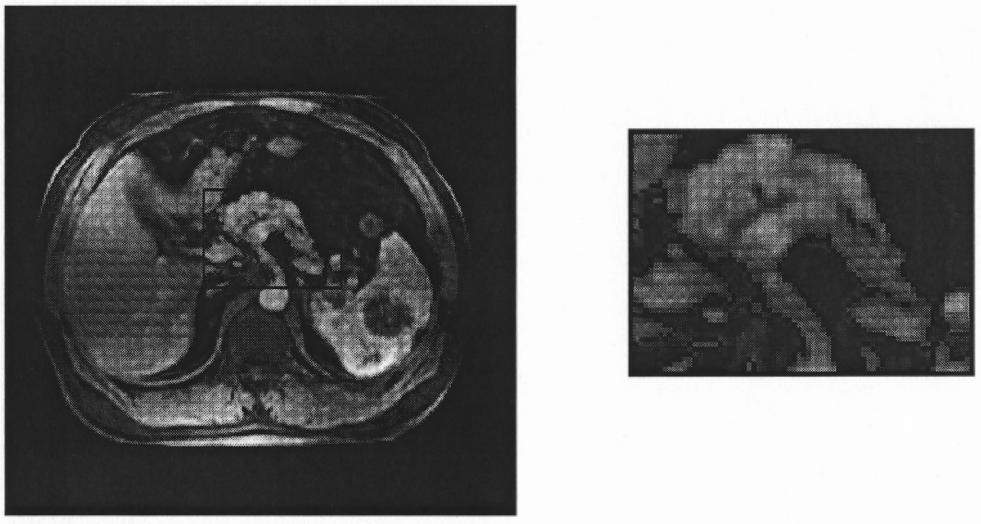

(a) (b)

**Figure 4.3** An axial MR slice of the abdomen. (a) Pancreas segmented using 2 clusters, (b) Enlarged view of the segmented pancreas.

Figure 4.4a and 4.4b show the result of segmenting the pancreas from the abdominal CT image volumes. Here again, only the results in one representative slice of the pancreas is shown. The number of clusters chosen here was also two, based on the image histogram of the selected region obtained. It can be observed in Figure 4.4a that due to very little variation in intensities of the pancreatic regions and its neighboring

structures, the contours of the regions bordering the pancreas were also detected in addition to the contour of the pancreas.

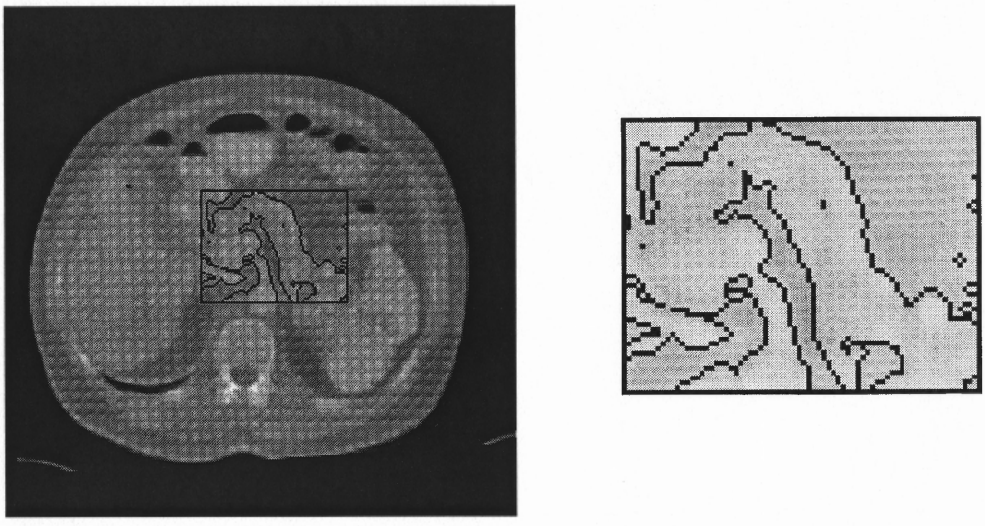

(a) (b)

**Figure 4.4** An axial CT slice of the abdomen, (a) Pancreas segmented using 2 clusters. (b) Enlarged view of the segmented pancreas.

Figures 4.5 and 4.6 show results of segmenting the pancreas from the MR and CT image volumes after gaussian white noise (with mean = 0 and variance = 0.001) was added to the images. The pancreas segmented from the noisy images was compared with that obtained from the actual images and the variation between the two clusters containing the pancreas was calculated. This gave an objective criterion about the performance of the segmentation algorithm in the presence of noise. For the noisy MR image shown in Figure 4.5a, the percentage non-overlap of pixels between the pancreas segmented before and after addition of noise respectively was 0.01. For the noisy CT image shown in Figure 4.6a, the percentage non-overlap of pixels between the pancreas

segmented before and after addition of noise respectively was 0.089. Thus, the segmentation had little statistical difference in the variation between clusters before and after the addition of noise. Further, the performance of the procedure was better in noise-corrupted MR images compared to the noise-corrupted CT images, due to the greater sensitivity of MRI to the various tissue types.

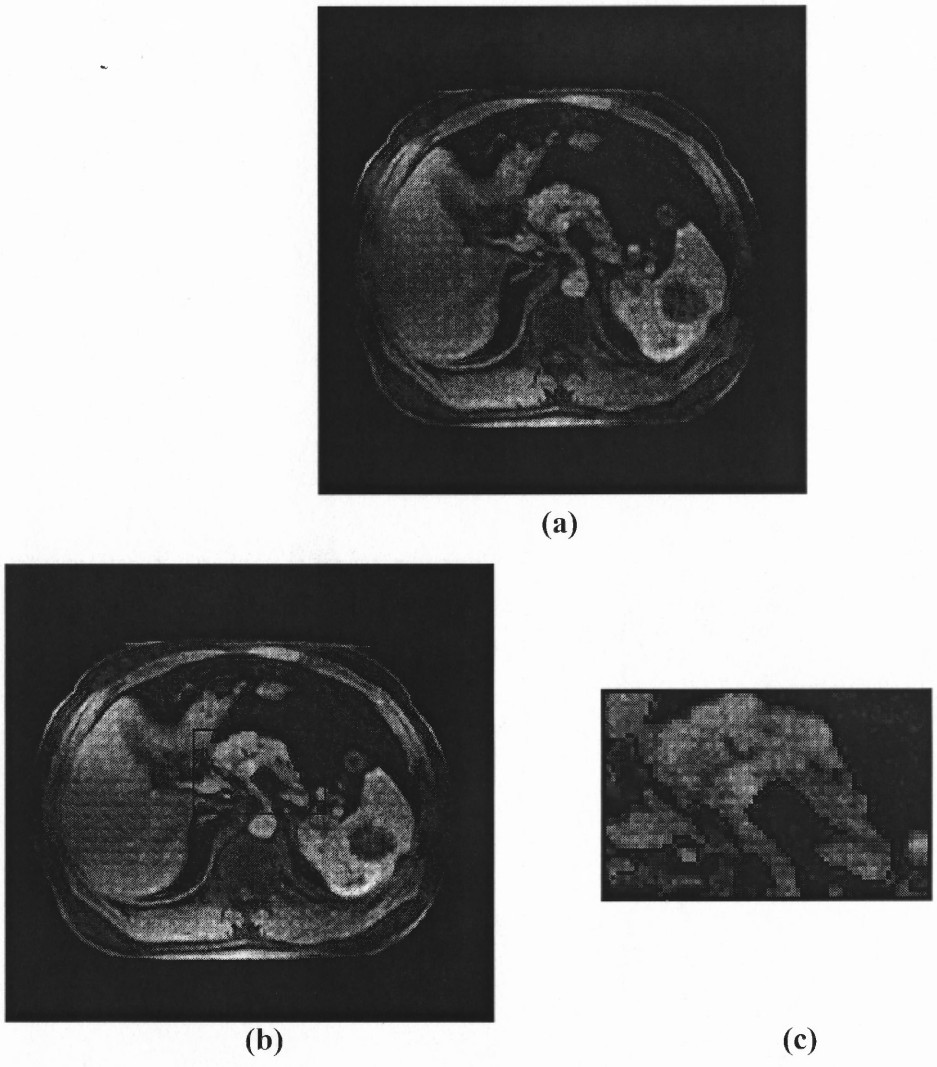


**Figure 4.5** (a) An axial MR slice of the abdomen corrupted with a gaussian noise having zero-mean and variance = 0.001, (b) Pancreas segmented from the noise-corrupted image (number of clusters chosen as 2). (c) Enlarged view of the segmented pancreas.

(a)

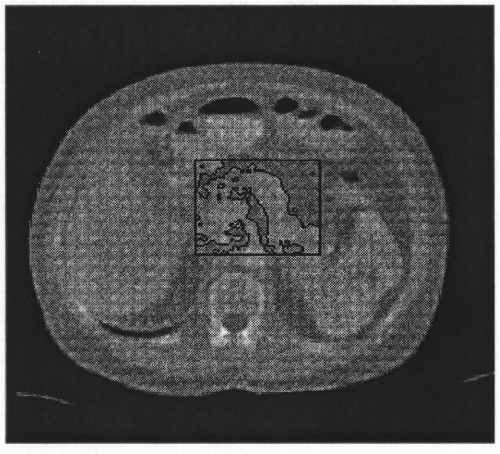

(b)

(c)

**Figure 4.6** (a) An axial CT slice of the abdomen corrupted with a gaussian noise having zero-mean and variance = 0.001, (b) Pancreas segmented from the noise-corrupted image (number of clusters assumed was 2), (c) Enlarged view of the segmented pancreas.

An increase in the noise variance added to the image results in an increase in the dispersion of the histogram of the image. In other words, more noise variance would mean more variance of the image intensity values from the average value. The effect of noise variance on the segmentation process is illustrated in Figure 4.7. The percentage of non-overlapping pixels between the pancreas segmented from the actual image and the

pancreas segmented from the noise-corrupted image was determined for various intensity levels of noise added to the images. The results showed that the percentage non-overlap increased with increase in the noise variance. It is evident from Figure 4.7 that this increase was more pronounced in the CT images compared to the MR images.

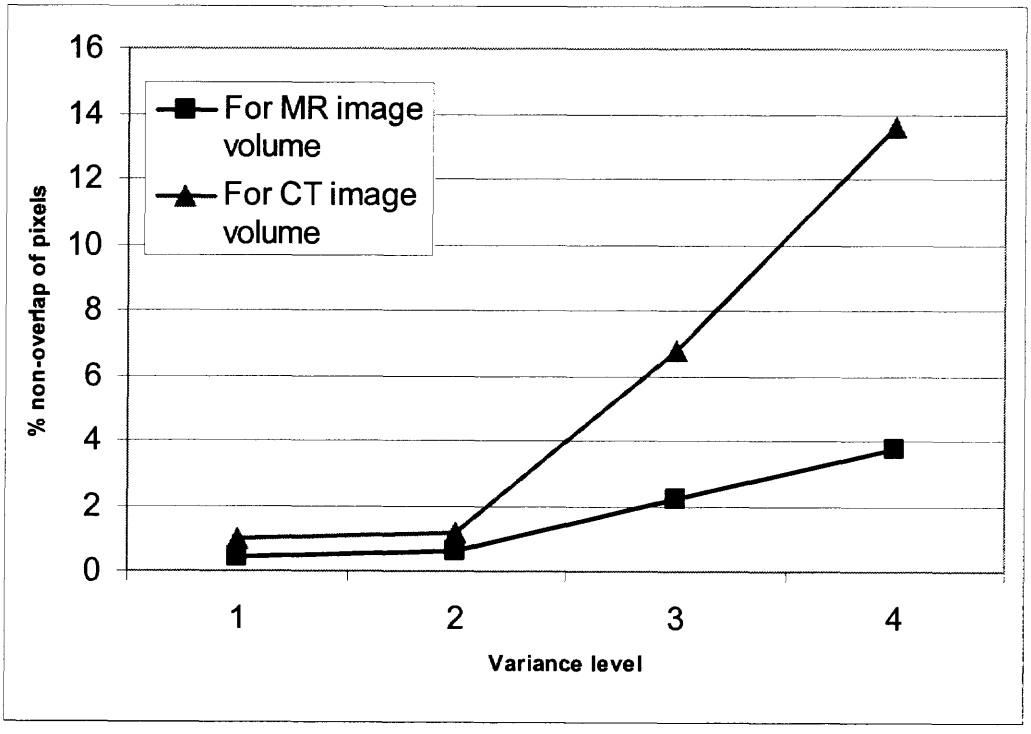


**Figure 4.7** Plot showing the percentage misalignment with increase in variance values. (Variance level 1 = 0.0001, 2 = 0.001, 3 = 0.01, 4 = 0.1 respectively on the X axis)

Figures 4.8 and 4.9 show the comparison between a manually traced contour and the contour as detected by the segmentation procedure. Even though the manual tracing method is not an efficient technique, it gives an approximate idea of the effectiveness of the segmentation procedure for detecting the pancreas. Figure 4.8a and 4.8c show the manually traced contour and the contour as detected by the segmentation procedure for an MR image respectively. Figure 4.8b and 4.8d show the enlarged version of the results

obtained in 4.8a and 4.8c respectively. Figure 4.9a and 4.9c show the same results for a CT image with the enlarged version being represented by Figures 4.9b and 4.9d. It can be visually perceived that both the segmented regions are almost alike except for some background noise pixels in the results obtained by the segmentation procedure.

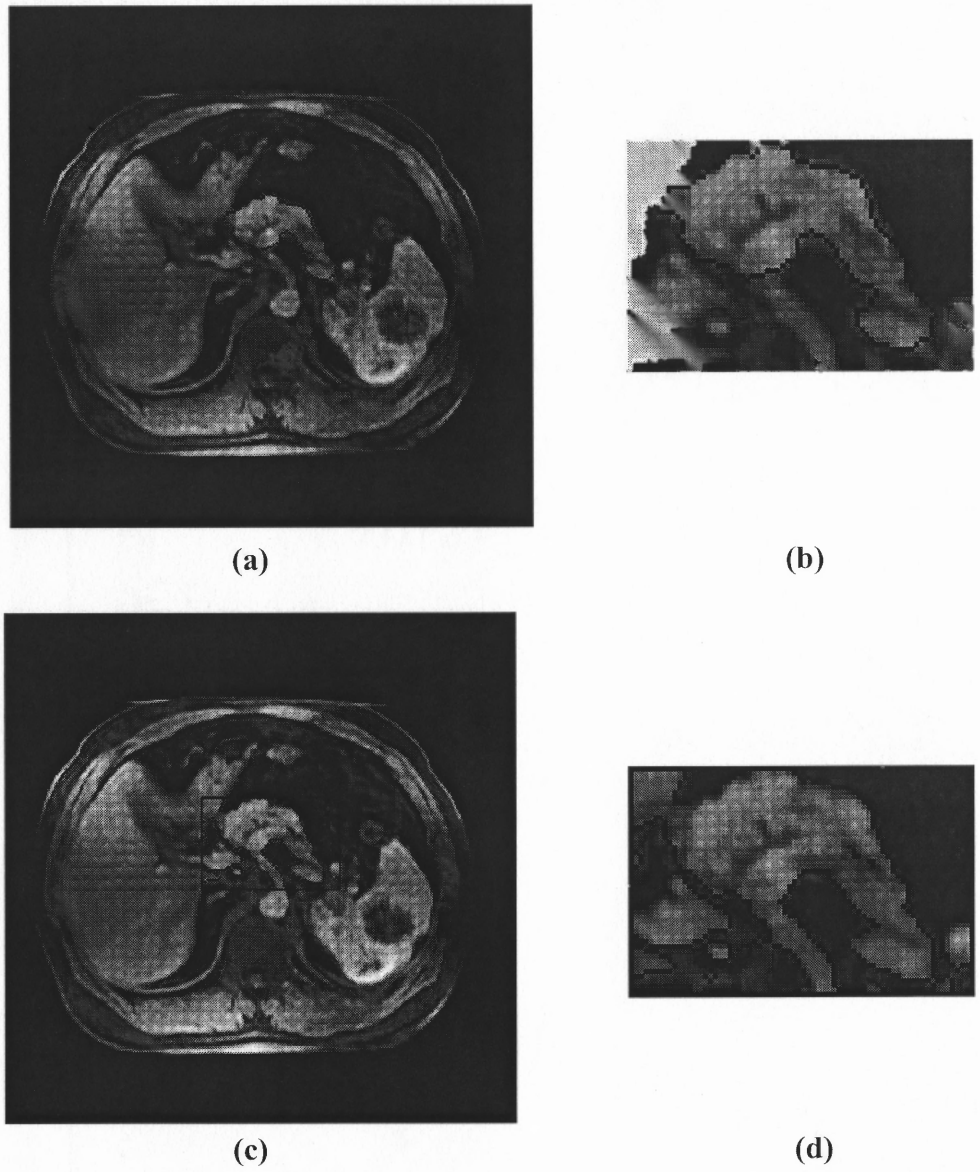


**Figure 4.8** Axial MR slice (a) Pancreas contour traced out by hand, (b) Enlarged view, (c) Pancreas contour traced out by the segmentation procedure, (d) Enlarged view.

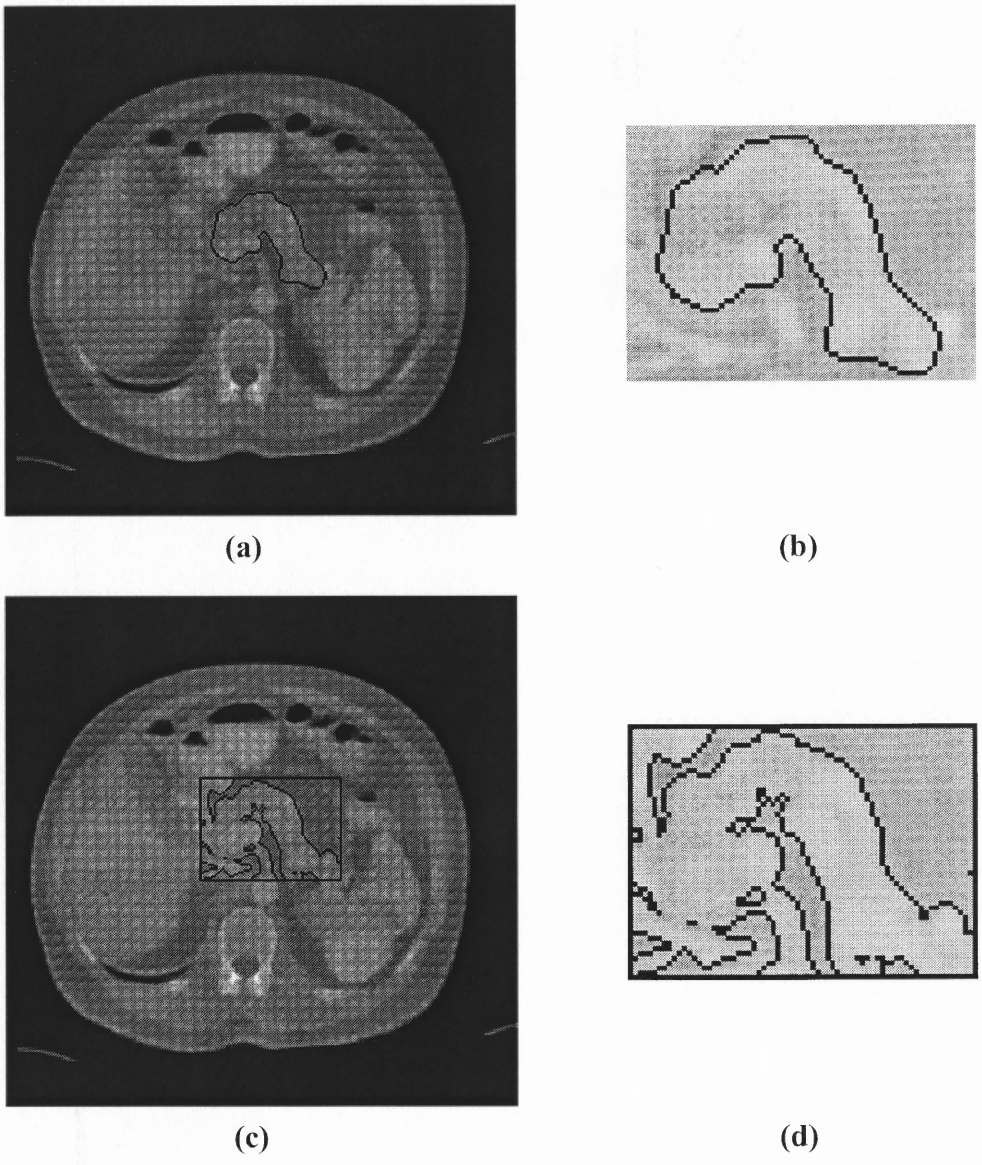


**Figure 4.9** Axial CT slice (a) Pancreas contour traced out by hand, (b) Enlarged view, (c) Pancreas contour traced out by the segmentation procedure, (d) Enlarged view.

Table 4.1 lists the average percentage overlap (obtained by measuring the number of overlapping pixels) between the manually-traced pancreas contour and the pancreas contour as detected by the segmentation procedure, for the different MR datasets. The overlap between the manually–traced contour and the contour detected by the

segmentation procedure was determined for three different trials per dataset. Based on these values the average percentage overlap (mean ± standard deviation) was found.

A comparison was also made between the manually-traced contour and a contour generated by the segmentation procedure for the image corrupted with a zero-mean gaussian random noise of variance 0.01. In the case of noisy datasets, 100 trials were performed where in each trial a different gaussian random noise distribution (having mean = 0 and variance = 0.01) was added to the image. For each case, the pancreas contour was detected using the segmentation method and was compared with a manually-traced contour as obtained from the image before noise was added to it. The mean ± standard deviation value of the average percentage overlap in all the five MR datasets before addition of noise was 98.23 ±0.089 and after addition of noise was 97.95 ±0.002. Similar comparisons were also done for the CT images. Table 4.2 shows the results for CT datasets. The mean ± standard deviation value of the average percentage overlap in all the five CT datasets before addition of noise was 98.30 ±0.082 and after addition of noise was 97.79 ±0.002. These values show that the method is less sensitive to low-variance noise, statistically.

**Table 4.1** Average Percentage of Overlapping Regions for Hand-drawn Contour and Contour Generated by the Segmentation Procedure for an MR Image Volume

| | **Average percentage overlap of segmented pancreas** | |
|---|---|---|
| | Without noise | With noise |
| Dataset 1 | 98.46 ±0.071 | 98.19 ±0.003 |
| Dataset 2 | 97.74 ±0.166 | 97.49 ±0.002 |
| Dataset 3 | 98.30 ±0.061 | 98.21 ±0.002 |
| Dataset 4 | 98.61 ±0.096 | 98.32 ±0.001 |
| Dataset 5 | 98.06 ±0.050 | 97.53 ±0.001 |

**Table 4.2** Average Percentage of Overlapping Regions for Hand-drawn Contour and Contour Generated by the Segmentation Procedure for a CT Image Volume

| | **Average percentage overlap of segmented pancreas** | |
|---|---|---|
| | Without noise | With noise |
| Dataset 1 | 98.21±0.123 | 97.78 ±0.003 |
| Dataset 2 | 98.33 ±0.108 | 97.63±0.004 |
| Dataset 3 | 98.90 ±0.067 | 98.27±0.002 |
| Dataset 4 | 97.86 ±0.087 | 97.16±0.001 |
| Dataset 5 | 98.22 ±0.026 | 98.13 ±0.002 |

Figures 4.10 and 4.11 shown below illustrate the noise sensitivity of the segmentation procedure, by measuring the percentage of overlap between the manually traced contour and the generated contour. It can also be inferred from the Figures that the noise sensitivity of the segmentation procedure is more pronounced in CT image volumes than in MR image volumes (by comparing the difference in the bars for each dataset in Figure 4.10 and 4.11 respectively).

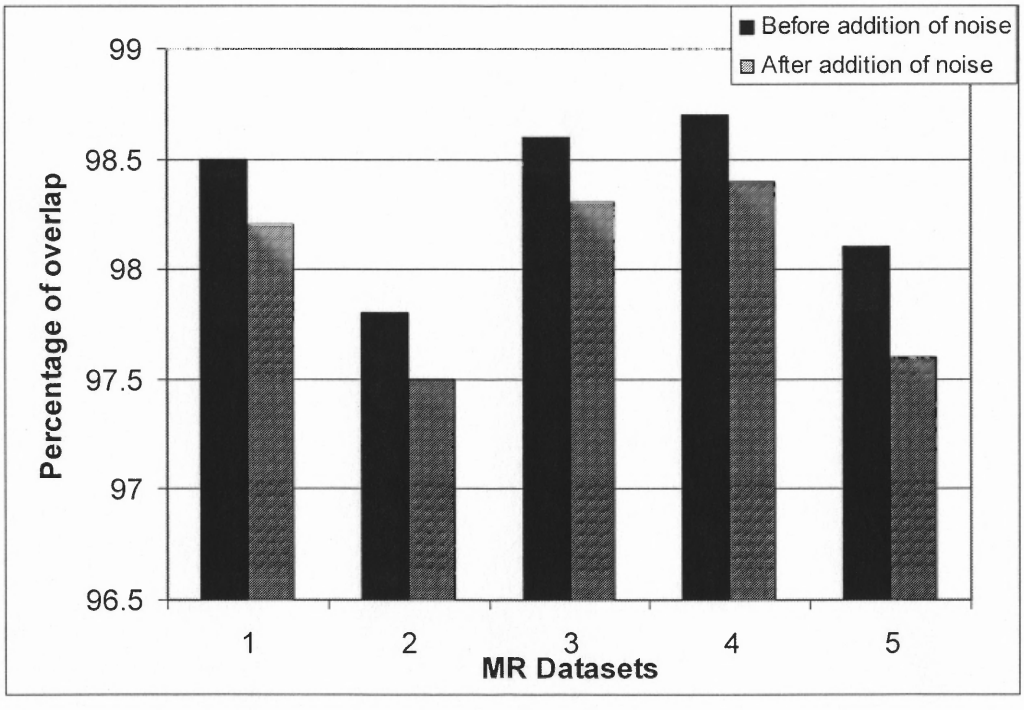


**Figure 4.10** Bar chart showing the percentage of overlap between manually drawn and hand traced contours, before and after noise addition for MR image volumes.

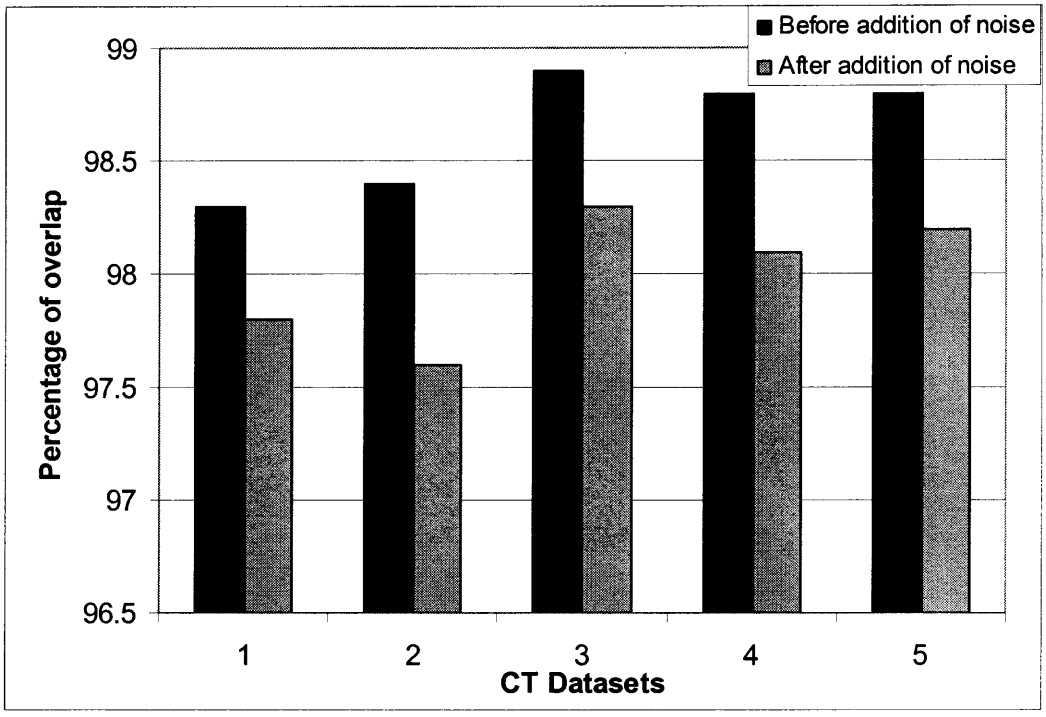


**Figure 4.11** Bar chart showing the percentage of overlap between manually drawn and hand traced contours, before and after noise addition for CT image volumes.

## 4.5 Detection of Pancreatic Cancer

Cancer in the pancreas is characterized by an abnormal size increase due to the presence of malicious tissue or tumors in the different pancreatic regions [24, 26]. Further, it has also been observed that these tumors are clustered together in particular sections of the pancreas (for eg: the head of the pancreas). Initial onset of pancreatic cancer is characterized by the manifestation of the cancer causing tumors in the various sections of the pancreatic mass. These tumors increase in size gradually thus also increasing the size of the pancreas, ultimately resulting in obstruction of the organs neighboring the pancreas.

Integration of information from MR and CT pancreatic volumes would help greatly to define the exact region and size of the pancreas in the abdomen. This would help determine any abnormal size increase in the pancreatic mass. Such integration can be done by simply aligning the images using the automatic registration algorithm developed in the present thesis. Once the information is integrated, the clustering based segmentation procedure can be used to cluster the pancreatic region and thus detect any malicious tissue (having intensity different than that of the pancreatic mass) within the pancreas. As the cancer causing tumors appear clustered in different sections of the pancreas, they can be easily detected by the segmentation procedure.

This was demonstrated using a test dataset on which the pancreas cancer tumor was simulated. This test dataset was obtained by combining the intensity information from a CT image volume and an MR image volume of the same abdominal region of a patient. Initially, these volumes were registered or aligned using the registration algorithm developed in this thesis. The aligned images were then added together to yield the integrated test dataset. The canceraceous tissue was then simulated as hyper-intensity voxels in the head of the pancreas. The tumor has a higher intensity value compared to the surrounding tissues and is clustered in the region. Practically, CT imaging of the abdomen using intravenous contrast agents might show such hyper-intensity tumors in the pancreas. However, sometimes the pancreatic mass itself might have high intensity values thus making the visual perception of the tumor difficult. In such cases, clustering would help detect the tumors. In the present thesis, the clustering-based segmentation procedure was used on this test dataset to trace out the pancreas as well as the simulated tissue within the head of the pancreas.

Figure 4.12 shows the integrated test image with a simulated tumor in the head region of the pancreas. Figure 4.13 shows the intensity distribution or the histogram of the entire pancreatic region. It is evident from Figure 4.13 that a bimodal distribution is obtained. The first distribution in the lower intensity range corresponds to the normal pancreatic mass and the second distribution in the higher intensity range corresponds to the canceraceous tumor.

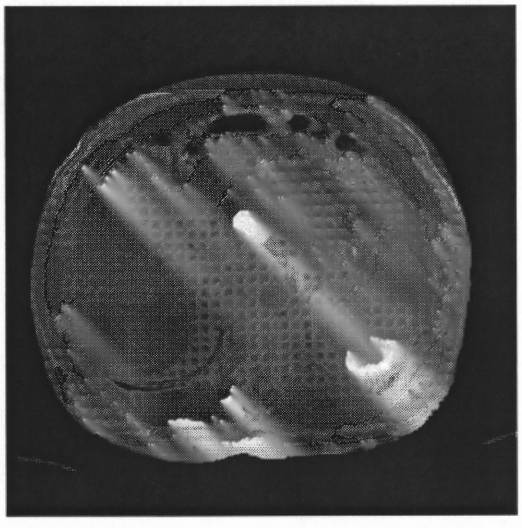

**Figure 4.12** Cancer tumor simulated in the head of the pancreas, in a CT-MR integrated test image.

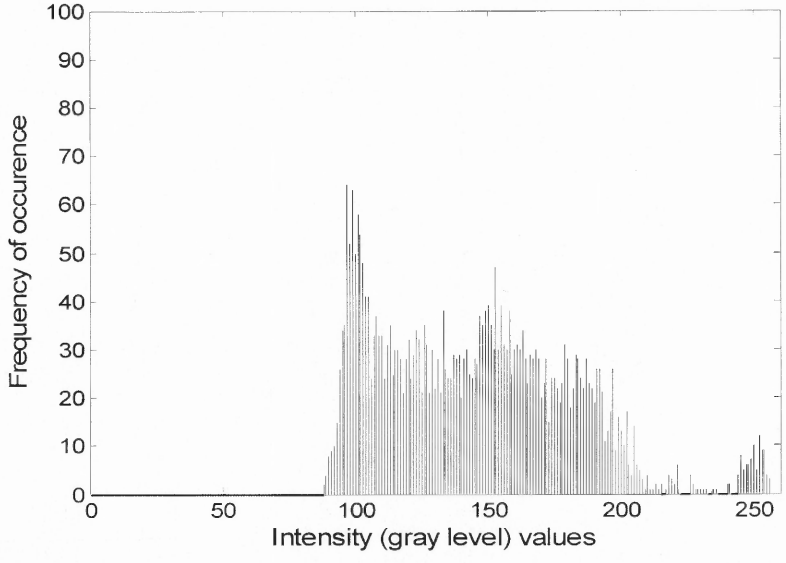


**Figure 4.13** Histogram of the pancreatic region with a simulated tumor in the head of the pancreas.

Figure 4.14a and 4.14b show the results of the tumor as detected by the segmentation procedure. In Figure 4.14b, the pancreas contour was also traced and this image was overlaid on the tumor contour traced image (4.14a) to achieve the end result.

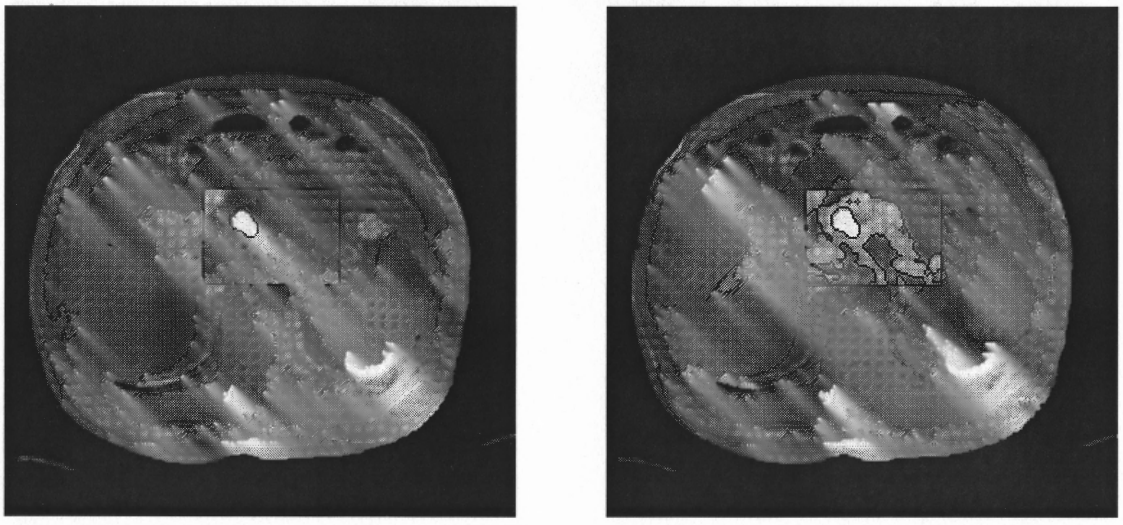

(a) (b)

**Figure 4.14** Simulated tumor in the pancreas head as detected by the segmentation procedure.

# CHAPTER 5

# DISCUSSION AND CONCLUSIONS

Due to the low survival rate (< 5%) and high mortality rates caused by pancreas cancer in the recent years, an effective diagnostic tool for early detection of the cancer becomes imperative. Improvements in medical imaging technologies have resulted in well-defined images of the abdomen, showing intricate details of its internal organs. Due to patient breathing and its proximity to the lungs, the relative location of the pancreas changes significantly with the respiration cycle. A comparison of the progression of the cancer or treatment evaluation requires precise localization of the pancreas. Within subject registration is imperative for comparison of the pancreas for both within-session and between-session analyses. Once the motion artifacts are corrected, the pancreatic region can be segmented and analyzed for cancer progression or treatment evaluation in an automatic fashion.

Also, different imaging modalities highlight different complimentary features in the radiological images obtained. For example, MR images of the abdomen are sensitive to fat and the various tissues of the intra-abdominal organs and hence the MR images can distinguish the pancreas with its neighboring regions effectively. CT images however, show intricate details about the pancreatic mass, but in most of the images there is no significant intensity difference between the pancreas and its neighboring organs. Hence, if the information from both these modalities can be integrated, a more information can be obtained that will facilitate detailed analysis of the pancreas.

An intensity based registration algorithm was developed in the present thesis for the exact localization of the pancreas and for also aligning two inter-modality images and thus obtain the required information from the aligned image. The registration algorithm was automatic and required only initial inputs. Once registered or aligned, the analysis of the pancreas was done by a clustering-based segmentation procedure. The segmentation procedure initially clustered the image and generated a contour around the region of interest (pancreatic region), thus segmenting it.

The registration and segmentation based processing method developed in the present thesis for the detection of pancreatic cancer is novel due to a number of factors. Currently only a few registration and segmentation procedures exist independently for 3D abdominal images, and as a consequence an effective integrated procedure for pancreas cancer screening and evaluation is lacking. The methodology developed here is one such integrated procedure for detection of pancreatic cancer. The algorithm can also account for shear and scaling in addition to translation and rotation (valid only for rigid body).

The major advantage of the mutual information (MI) based automatic registration method is that the MI is a statistical measure. Also, the MI value depends only on the relative occurrence of similar intensity voxels. The marginal entropy used in computation of mutual information avoids the error due to the image background overlap, which occurs frequently while computing the joint entropy. Hence mutual information is more accurate than joint entropy or cross-correlation measures, which were used popularly in the past for intensity-based automatic registration algorithms [13].

The segmentation methodology presented also has numerous advantages. As the method solely depends on the image intensity values only, no sort of special data markers and other data manipulation techniques are necessary. The registration algorithm is dependent on the voxel intensity values in the corresponding sections of the images. The clustering based segmentation process also depends on the first-order features represented by the voxel intensity values and hence obviates the necessity of an image atlas or reference for sectioning out the region of interest. These factors contribute towards the simplicity of the algorithm.

The segmentation procedure generates a machine-drawn contour for desired regions of interest based on their intensity distribution. Such a procedure also reduces the time and labor to manually trace out contours from desired regions of interest, for analysis. Segmentation by clustering is less complex than vector-based methods [15-17] that also segment the images by tracing out the contours of the region of interest. Some of the popularly used vector-based methods for image segmentation can only detect specific contours and hence might not result in closed contours always [15, 16].

The overall algorithm is easy to implement (using MATLAB) in a commonly used image processing software and also easy to use. The methodology presented also enables users with minimal technical knowledge to use the algorithms efficiently.

The method developed has a few limitations also. The sub-voxel shifts in images were not considered while performing the registration procedure. Such sub-voxel shifts occurring in the images were rounded off to the nearest integer number during the registration process. As a consequence, sub-pixel registration cannot be performed. The sensitivity of the registration algorithm might also be affected to some extent due to the

image interpolation done in such cases. Also, the registration algorithm developed in the present work considers only the effect of an affine scaling and shearing on the images. Elastic deformations that have a minor effect on the images obtained were not considered in the present thesis.

Effective results were obtained in the present thesis using MR and CT images of the abdomen only. It is possible that the performance of the algorithm, when images from other modalities (PET for example) are used, may not be as reliable as the results obtained in the present case. Other pre-processing or special processing methodologies might have to be incorporated in the basic algorithm for obtaining satisfactory results in such cases. Also, more detailed studies on the effect of different types of noise on the images have to be done to further validate the efficiency of the algorithm.

A major application of the developed methodology would be in the screening and detection of pancreas cancer in its initial stages. Present methods for pancreas cancer detection have the ability to detect the cancer only beyond a certain stage when the lesions cannot be resected effectively. This is because of the progression of the cancer to the neighboring organs. Early detection of the cancer tissues would thus help to a great extent to surgical remove the lesions without causing any damage to the neighboring organs.

The methodology can also be used to study the effect of a drug on the cancer causing tissues, in the pancreas. This can be facilitated by tracking the progress of the cancer over a period of time, when the drug is being administered. Pre-surgical and post-surgical comparisons can also be done, in a similar manner. Such studies on cancer

progression in general, can be used for more effective research and development of therapeutic and curative procedures for pancreatic cancer.

The methodology developed can also be used for the analysis of other intra-abdominal organs, apart from the pancreatic region. This would help greatly in the screening of multiple organs in the abdomen for pathological conditions.

The overall methodology developed in the present work is thus an initial step for future developments in image processing methods for efficient prognosis and treatment of pancreatic cancer. The proposed method can be improved further by making it fully automatic and by including recent image processing techniques that can perform a more detailed analysis of the region of interest. With rapid developments in technology and image processing techniques, the future scope of such a method seems promising.

# APPENDIX A

# PRE-PROCESSING ALGORITHMS

The program codes listed in this appendix were used for the pre-processing of the raw MR and CT data.

## 1. Intensity adjustment routine *contraststch2.m*:

```
function [s6] = contraststch2(img,llim1,ulim1,llim2,ulim2)
%s6 = contraststch2(img,llim1,ulim1,llim2,ulim2)
%Convert original image to double using 'mat2gray'.
%Look at image histogram and specify the stretch limits
s = img; s2 = s;
%Intensity stretching between the specified limits
s3 = imadjust(s2,[0 llim1],[0 llim2]);
s4 = imadjust(s2,[llim1 ulim1],[llim2 ulim2]);
s5 = imadjust(s2,[llim1 1],[ulim2 1]);
%Adjusting the overall image intensity using the 'stretched' values
s6 = zeros(256,256);
for l11 = 1:256
for l12 = 1:256
if s2(l11,l12) >= 0 &&  s2(l11,l12) < llim1
s6(l11,l12) = s3(l11,l12);
end
end
end
sx = s6;
for l21 = 1:256
for l22 = 1:256
if s2(l21,l22) >= llim1 && s2(l21,l22) < ulim1
s6(l21,l22) = s4(l21,l22);
end
end
end
sy = s6;
for l31 = 1:256
for l32 = 1:256
if s2(l31,l32) >= ulim1 && s2(l31,l32) <= 1
s6(l31,l32) = s5(l31,l32);
end
end
end
```

## 2. Slice stacking routine *hvolalign.m*:

```
function [aligndvol] = hvolalign_reloaded(imgvol,refrimg)
%[aligndvol] = hvolalign_reloaded(imgvol,refrimg)
%
%HIERARCHIAL REGISTRATION - registered portion of the volume image is
%used as the reference volume for the next stage of registration. If
%'refrimg' is not specified, the FIRST slice is taken as the reference
%initially and registration proceeds successively. The function can be
%used for registering successive 'n' sliced volumes also within the
%same image volume
%
%imgvol = the actual image volume
%refrimg = reference slice / slices
%aligndvol = the aligned (motion corrected) image slices

%Initialization
[xv yv zv] = size(imgvol);
aligndvol = zeros(xv,yv,zv);
if nargin == 1, refrimg = imgvol(:,:,1); end
```

```
[xr yr zr] = size(refrimg);
reffimg = refrimg;
ns = zv/zr;
%Heirarchial alignment of slices
for lindx = 1:ns
%Selecting the next consecutive slice(s)
zd2 = zr*lindx;
zd1 = zd2 - (zr-1);
targtimg = zeros(xr,yr,zr);
targtimg = imgvol(:,:,zd1:zd2);
%Registration step
[rref,acttgt,lintgt,afftgt,finaltgt2]= reg3d_nslice(reffimg,targtimg);
aligndvol(:,:,zd1:zd2) = finaltgt2;
reffimg2 = reffimg;
reffimg = zeros(xr,yr,zr);
reffimg = finaltgt2;
end
```

# APPENDIX B

# REGISTRATION ALGORITHMS

The program codes listed in this appendix were used for the registration of intra-modality (CT with CT or MR with MR) and inter-modality images (CT with MR) of the abdomen.

## 1. Main function and sub-functions used for intra-modality registration:

```
function [rreffinl,acttgt,lintgt,afftgt,finaltgt,parm1, ...
                par2,rang,gues_a,pps2] = reg3d_nslice(rfimg,tgimg)
%[rref,acttgt,lintgt,afftgt,finaltgt,parm1,par2,rang,gues_a,pps2] =
%reg3d_nslice(rfimg,tgimg);
%
%INPUT:
%rfimg => reference volume
%tgimg => target volume
%
%OUTPUT:
%rref => The reference volume
%acttgt => The target volume
%lintgt => Target volume after linear-shift correction
%afftgt => Target volume after affine correction
%finaltgt => Final registered image
%parm1 => Linear shift correction parameters
%par2 => Affine shift correction parameters
%rang => Rotational shift correction parameters

reffimg = rfimg;
targtimg = tgimg;

%LINEAR SHIFT CORRECTION
ttimg2 = targtimg;
%Zero padding the target image
[xs ys zs] = size(ttimg2); vdat3 = zeros(xs+256,ys+256,zs+8);
vdat3(128:xs+127,128:ys+127,4:zs+3) = ttimg2;
clear xs ys zs;
%Estimating initial guess values for the simplex
guues = initialestimate3d(reffimg,ttimg2);
%Linear shift correction by optimization
[rref rtgt parm1] = transl_corrctn3d(reffimg,vdat3,guues);

%AFFINE TRANSFORMATION CORRECTION
%Zero padding reference image (size increased to 512x512)
[x y z] = size(rref);
tempp = zeros(512,512,z); [a b c] = size(tempp);
x1 = round((a-x)/2); y1 = round((b-y)/2);
x2 = (x1+x)-1; y2 = (y1+y)-1;
tempp(x1:x2,y1:y2,1:z) = rref(:,:,1:z);
clear rref; rref = tempp;
%Affine shift correction by optimization
initial_gues = [1 1 0];
[rref2 rtgt2 par2 pps2] = re_affine3d(rref,rtgt,initial_gues);

%ROTATIONAL SHIFT CORRECTION
%Estimating the guess value for rotation
gues_a = guessangl2new(rref2,rtgt2);
%Rotational shift correction by optimization
[rref3,rtgt3,rang] = rot_correctn3d(rref2,rtgt2,gues_a);

%Image resizing to facilitate display (resizeimg.m was a code developed %to resize an image to
512 x 512 if no input size value %is specified)
lintgt2 = resizeimg(rtgt); afftgt2 = resizeimg(rtgt2);
finaltgt2 = resizeimg(rtgt3);
```

```
rreffinl = rref2(128:383,128:383,:); %Reference image
acttgt = targtimg;                %Target image
lintgt = lintgt2(128:383,128:383,:); %Target image after linear-shift
                                                    %correction
afftgt = afftgt2(128:383,128:383,:); %Target image after affine-shift
                                                    %correction
finaltgt = finaltgt2(128:383,128:383,:); %Final target image after
                                                %rotational-shift correction
%-----------------------------------------------------------------------------------------------------------------
%Function to determine linear-shift guess values
function [guess]=initialestimate3d(orig,mdimg)
[cx1,cy1,cz1,image1,l1]=centroid3dimage(orig); %Centroid of image 1
[cx2,cy2,cz2,image2,l2]=centroid3dimage(mdimg); %Centroid of image 2
guess(1)=round((cx2-cx1)); %Difference in X,Y,Z centroid points
guess(2)=round((cy2-cy1));
guess(3)=round((cz2-cz1));
end
%-----------------------------------------------------------------------------------------------------------------
%Centroid computation function used above
function [centx, centy,centz]=centroid3dimage(image1)
[r c h]=size(image1);
image1=mat2gray(double(image1));
%Convert image to Black and White
for i=1:h
bwimage(:,:,i)=double( im2bw(image1(:,:,i),graythresh(image1)));
end
cx=0;cy=0;cz=0;
[r c h]=size(image1);
area=0;
%Compute centroid based on surface area
for k=1:h
for i=1:r
for j=1:c
area=area+bwimage(i,j,k);
cx=cx+i*bwimage(i,j,k);
cy=cy+j*bwimage(i,j,k);
cz=cz+k*bwimage(i,j,k);
end
end
end
centx=cx/area; centy=cy/area; centz=cz/area;
end
%-----------------------------------------------------------------------------------------------------------------
%Function for linear-shift correction
function [refimg2,tarimg2,parm]=transl_corrctn3d(refi1,targi1,gs1)
refffimg1 = refi1; tarrgimg1 = targi1; init_guess = gs1;
%Set optimization options
options = optimset('MaxFunEvals',40000,'Display','on');
%Optimization by down-hill simplex method
[igss2, fval] = fminsearch('rescaletrans3d',init_guess,options, ...
                                    refffimg1,tarrgimg1);
%Final alignment of the image
[n1 n2 n3]=size(refffimg1); xt=1:n1; yt=1:n2; zt=1:n3;
xx=round(xt+127+igss2(1)); yy=round(yt+127+igss2(2));
zz=round(zt+3+igss2(3));extrcted=(tarrgimg1(xx, yy, zz));
refimg2 = refffimg1; tarimg2 = extrcted; parm = igss2;
```

```
%-----------------------------------------------------------------------------------------------------------------
%Optimization routine for linear-shift correction
function terr = rescaletrans3d(guesst, Im1, Im2)
actu = Im1; reqd = Im2; ings = guesst;
[n1 n2 n3]=size(actu);
%Extract the required portion of the image alone
xt= 1:n1; yt= 1:n2; zt= 1:n3;
xx=round(xt+127+ings(1));
yy=round(yt+127+ings(2));
zz=round(zt+3+ings(3));
reqd2 =(reqd(xx, yy, zz));
%Calculate the normalized Mutual information--parameter to be optimized
NMI=normMI3d(actu,reqd2);NMII=-NMI; terr = NMII;
%-----------------------------------------------------------------------------------------------------------------
%Function for affine correction
function [refimg1,tarimg1,pts1,ps2] = re_affine3d(refi,targi,igs)
I = refi; I_transform = targi;
% Find transformation to realign image
initial_scale = igs;       % Set initial guess
%Set optimization options
options = optimset('MaxFunEvals',10000,'Display','on');
%Optimization by down-hill simplex method
[scale,FVAL] = fminsearch('rescale3d',initial_scale,options, ...
                                                I,I_transform);
ps2 = [scale(1),scale(2),scale(3)];
% Realign image using optimized scaling
if scale(1) > 1.15
scale(1) = 1.05;
elseif scale(1) < 0.8
scale(1) = 0.9;
end
if scale(2) > 1.3
scale(2) = 1.2;
elseif scale(2) < 0.85
scale(2) = 0.95;
end
disp(scale);
X = [scale(1) scale(3) 0; 0 scale(2) 0; 0 0 1];
Tform = maketform('affine',X);
I_aligned = imtransform(I_transform,Tform);
refimg1 = refi; tarimg1 = I_aligned;
pts1 = [scale(1),scale(2),scale(3)];
%-----------------------------------------------------------------------------------------------------------------
%Optimization routine for affine correction
function err = rescale3d(scale, I, I_transform)
%Set limits for affine scaling values
if scale(1) >= 1.4,scale(1) = 1;end
if scale(2) >= 1.4,scale(2) = 1;end
if scale(1) <= 0.7,scale(1) = 1;end
if scale(2) <= 0.7,scale(2) = 1;end
% Perform transformation
X = [scale(1) scale(3) 0; 0 scale(2) 0; 0 0 1];
Tform = maketform('affine',X);
I_aligned = imtransform(I_transform,Tform);
%Calculate the normalized Mutual information-parameter to be optimized
NMI=normMI3d(im2double(I),im2double(I_aligned));
```

```
NMII=-NMI; err = NMII;
%-----------------------------------------------------------------------------------------------------------
%Function to calculate guess value for angular shift correction
function g_ang = guessangl2new(imgrr,imgtt)
[x1 y1 z1] = size(imgrr); [x2 y2 z2] = size(imgtt);
if z1==1 || z1==2 %Take whole volume as reference image if it has only
%1 or 2 slices only
imgr = imgrr; imgt = resizeimg(imgtt,512,512);
else
%Take the median 3 slices from actual reference and target volumes for
%estimating the guess angle
a2 = ceil(z1/2); b2 = ceil(z2/2);
a1 = a2-1; a3 = a2+1; b1 = b2-1; b3 = b2+1;
imgr = imgrr(:,:,a1:a3);
imgt = imgtt(:,:,b1:b3);
imgt = resizeimg(imgt,512,512);%Resize image to twice the original size
end
imgt2 = zeros(size(imgt)); g_ang1 = zeros(1,2);
mmival = zeros(1,10);
%Assume that the max angular rotation is 10 deg and min is 1 deg
for i = 1:10
imgt2 = imrotate(imgt,-i,'bilinear','crop');
mmival(i) = normMI3d(imgr,imgt2); %Calculate NMI for each rotation
clear imgt2;
end
m1 = max(mmival);
[d1,d2] = find(mmival==m1); %Find the maximum NMI value
g_ang1(1) = -d2;
%Repeat the above steps for clockwise rotation of image also
clear d1 d2; mmival = zeros(1,10); imgt2 = zeros(size(imgt));
for i = 1:10
imgt2 = imrotate(imgt,i,'bilinear','crop');
mmival(i) = normMI3d(imgr,imgt2);clear imgt2;
end
m2 = max(mmival);[d1,d2] = find(mmival==m2);
g_ang1(2) = d2;clear d1 d2;
%Fix guess angle value as the angular rotation that yielded the maximum %NMI value
if m1>m2
g_ang = [0,0,g_ang1(1)];
else
g_ang = [0,0,g_ang1(2)];
end
%-----------------------------------------------------------------------------------------------------------
%Function for rotational shift correction
function [refimg2,tarimg2,angll]=rot_correctn3d(refi1,targi1,ga)
refffimg = refi1; tarrgimg = targi1; guessang = ga;
%Set optimization parameters
options = optimset('MaxFunEvals',40000,'Display','on');
%Optimization by down-hill simplex method
[angl2, fval] = fminsearch(@rescaleang3d,guessang,options, ...
                                    refffimg,tarrgimg);
disp(-fval);
angl2(1) = 0;angl2(2) = 0;
prextrct=i3drotate(tarrgimg,angl2(1),angl2(2),angl2(3));
refimg2 = refffimg; tarimg2 = prextrct; angll = angl2;
%-----------------------------------------------------------------------------------------------------------
```

```
%Optimization for rotational shift correction
function aerr = rescaleang3d(guessang, I1, I_transform1)
actu = I1;rottd = I_transform1;ga2 = guessang;
ga2(1) = 0; ga2(2) = 0; %Rotation abt Z only
rotatedd = i3drotate(rottd,ga2(1),ga2(2),ga2(3));%Re-rotate the image
%Calculate the Mutual information
NMI=normMI3d(actu,rotatedd);NMII=-NMI; aerr = NMII;

function [imgg] = i3drotate(img,angx,angy,angz)
%For future incorporation of shear along X and Y
if angx ~= 0 || angy ~= 0
img1 = fft3dshearx(img,angx); %Shear along X - Future development
img2 = fft3dsheary(img1,angy);%Shear along Y - Future development
img3 = imrotate(img2,angz,'bilinear','crop');
else
img3 = imrotate(img,angz,'bilinear','crop');
end
imgg = img3;
```

## 2. Function for Mutual Information calculation *normMI3d.m*:

```
function NMI=normMI3d(referenced,extractedimage)
%Zero-pad target image to 512x512
[x y z] = size(extractedimage);
tempp = zeros(512,512,z);
[a b c] = size(tempp);
x1 = round((a-x)/2);y1 = round((b-y)/2);
x2 = (x1+x)-1;y2 = (y1+y)-1;
tempp(x1:x2,y1:y2,1:z) = extractedimage;
clear extractedimage;
extractedimage = tempp;
us_referenced=im2uint8(mat2gray(double(referenced)));
us_extractedimage=im2uint8(mat2gray(double(extractedimage)));
%Define size of joint histogram
rows=size(us_referenced,1);
cols=size(us_extractedimage,2);
height=size(us_referenced,3);
N=256; h=zeros(N,N);
%FIND JOINT HISTOGRAM
for kk=1:height
for ii=1:rows
for jj=1:cols
h(us_referenced(ii,jj,kk)+1,us_extractedimage(ii,jj,kk)+1)...
        = h(us_referenced(ii,jj,kk)+1,us_extractedimage(ii,jj,kk)+1)+1;
end
end
end
[r,c] = size(h);
b= h./sum(h(:)); % normalized joint histogram
y_marg=sum(b); %sum of the rows of normalized joint histogram
x_marg=sum(b');%sum of columns of normalized joint histogran
%Calculate the marginal entropy values
Hy=0;
for i=1:c;
if( y_marg(i)==0 )     %do nothing
else
```

```
Hy = Hy + -(y_marg(i)*(log2(y_marg(i)))); %marginal entropy for image 1
end
end
Hx=0;
for i=1:r;
if( x_marg(i)==0 )%do nothing
else
Hx = Hx + -(x_marg(i)*(log2(x_marg(i)))); %marginal entropy for image 2
end
end
h_xy = -sum(sum(b.*(log2(b+(b==0))))); % joint entropy
MI=(Hx+Hy-h_xy);% Mutual information
NMI=[(MI/h_xy)+1]; %Normalized MI
```

### 3. Main function and sub-functions used for inter-modality registration:

```
function [slcs,new_reffimg3,new_targtimg4,reg_targt,finaltgt, ...
          finaltgt2] = newregalgorithm4(reffimg,rsmm,targtimg,tsmm)
reffimg1 = sliceresizer(reffimg,rsmm);
targtimg1 = sliceresizer(targtimg,tsmm);
%Select the three median slices
z1 = size(targtimg1,3);z2 = size(reffimg1,3);
zz2 = round(z1/2);zz1 = zz2-1;zz3 = zz2+1;
targtimg2 = targtimg1(:,:,zz1:zz3);
%Registration at reduced resolution
warning('off');
t = [0.5 0 0; 0 0.5 0; 0 0 1];
tform = maketform('affine',t);
reffimg2 = imtransform(reffimg1,tform);
targtimg3 = imtransform(targtimg2,tform);
[slcs] = newregalgorithm(reffimg2,targtimg3);
%Slices above and below median of the target image
sa = zz2; %Above
sb = z1-sa; %Below
%Slices above and below the registered median line of reference
sa1 = slcs(1)+1; %Above
sb1 = z2-sa1; %Below
%For top-half
if sa1-sa > 0 %positive - chop reference image
reffimg31 = reffimg1(:,:,(sa1-sa)+1:sa1);
targtimg41 = targtimg1(:,:,1:sa);
elseif sa1-sa < 0 %negative - chop target image
reffimg31 = reffimg1(:,:,1:sa1);
targtimg41 = targtimg1(:,:,(sa-sa1)+1:sa);
else          %both are equal
reffimg31 = reffimg1(:,:,1:sa1);
targtimg41 = targtimg1(:,:,1:sa);
end
%For bottom-half
if sb1-sb > 0 %positive - chop reference image
reffimg32 = reffimg1(:,:,(sa1+1):(z2-(sb1-sb)));
targtimg42 = targtimg1(:,:,sa+1:z1);
elseif sb1-sb < 0 %negative - chop target image
reffimg32 = reffimg1(:,:,sa1+1:z2);
targtimg42 = targtimg1(:,:,(sa+1):(z1-(sb-sb1)));
```

```
else            %both are equal
reffimg32 = reffimg1(:,:,sa1+1:z2);
targtimg42 = targtimg1(:,:,sa+1:z1);
end
%Combine both halves appropriately to show the matched portion
z31 = size(reffimg31,3); z32 = size(reffimg32,3);
reffimg3(:,:,1:z31) = reffimg31;
reffimg3(:,:,z31+1:(z31+z32)) = reffimg32;
clear z31 z32;
z31 = size(targtimg41,3); z32 = size(targtimg42,3);
targtimg4(:,:,1:z31) = targtimg41;
targtimg4(:,:,z31+1:(z31+z32)) = targtimg42;
%Resizing ref & tgt images back to their original slice dimensions
[r1 c1 h1] = size(reffimg3); [r2 c2 h2] = size(targtimg4);
%Resizing the reference
fac1 = mod(h1,rsmm);
%If no of stray slices in ref volume is greater than half the %individual slice width then extrapolate
last slice to create a slice %of thickness = rsmm. If not just discard the stray slices
if fac1 >= round(rsmm/2)
for llp = 1:(rsmm-fac1)
reffimg3(:,:,h1+llp) = reffimg3(:,:,h1);
end
end
hh1 = size(reffimg3,3);fac2 = mod(hh1,rsmm);
arrsize = hh1-fac2;new_reffimg3 = zeros(r1,c1,(arrsize/rsmm));
count=1;
for kk = 1:rsmm:arrsize
ttemp = reffimg3(:,:,kk:(rsmm*count));
new_reffimg3(:,:,count) = sum(ttemp,3); %Leaves out the last few slices
count = count+1;
end
clear fac1 fac2 llp arrsize kk
%Resizing the target
fac1 = mod(h2,tsmm);
%If no of stray slices in ref volume is greater than half the %individual slice width then extrapolate
last slice to create a slice %of thickness = tsmm. If not just discard the stray slices
if fac1 >= round(tsmm/2)
for llp = 1:(tsmm-fac1)
targtimg4(:,:,h2+llp) = targtimg4(:,:,h2);
end
end
hh2 = size(targtimg4,3); fac2 = mod(hh2,tsmm);
arrsize = hh2-fac2; new_targtimg4 = zeros(r2,c2,(arrsize/tsmm));
count=1;
for kk = 1:tsmm:arrsize
ttemp = targtimg4(:,:,kk:(tsmm*count));
new_targtimg4(:,:,count) = sum(ttemp,3); %Leaves out the last few slices
count = count+1;
end
%Finally register the similar portions!
%But b4 that resize both volumes to have same no of slices.
%This is done by making the slice thickness of the volume having a %lesser slice thickness equal
to the slice thickness of the volume %having a greater slice thickness.
reg_reff = new_reffimg3;
reg_targt = sliceresizer4(new_targtimg4,tsmm,reg_reff,rsmm);
[rreffinl,finaltgt,lp,affp,rotp]= newregalgorithm5(reg_reff,reg_targt);
```

```
%Resize target back after registration
finaltgt2 = sliceresizer3(finaltgt,rsmm,tsmm);
%-----------------------------------------------------------------------------------------------------------
%Function1 to resize image slices
function [temparr1] = sliceresizer(targtimg,tsmm)
%mm -> Thickness of each individual slice of input image in mm
%This function returns an output image having slices of 1mm thick each.
%This is achieved by simple linear scaling and hence the output is only %an approximate
representation of the input.
[x1 y1 z1] = size(targtimg);
arrsize = round(z1*tsmm); %Total no of 1mm thick slices
temparr1 = zeros(x1,y1,arrsize);count = 0;
for ii = 1:z1
ctt = 0;
for jj = 1:tsmm
if round(tsmm) == tsmm
count = count+1;
temparr1(:,:,count) = targtimg(:,:,ii).*(1/tsmm);
elseif mod(ii,2) ~= 0 && ii ~= z1
count = count+1; ctt = ctt+1;
if ctt ~= floor(tsmm)
temparr1(:,:,count) = targtimg(:,:,ii).*(1/tsmm);
else
temparr1(:,:,count) = targtimg(:,:,ii).*(1/tsmm);
count = count+1;
temparr1(:,:,count) = targtimg(:,:,ii).*(0.5/tsmm) + ...
                              targtimg(:,:,ii+1).*(0.5/tsmm);
end
elseif mod(ii,2) == 0 && ii ~= z1
count = count+1;
temparr1(:,:,count) = targtimg(:,:,ii).*(1/tsmm);
elseif ii == z1
if mod(ii,2) == 0
count = count+1;
temparr1(:,:,count) = targtimg(:,:,ii).*(1/tsmm);
else
count = count+1; ctt = ctt+1;
if ctt ~= floor(tsmm)
temparr1(:,:,count) = targtimg(:,:,ii).*(1/tsmm);
else
temparr1(:,:,count) = targtimg(:,:,ii).*(1/tsmm);
count = count+1;
temparr1(:,:,count) = targtimg(:,:,ii).*(0.5/tsmm);
end
end
end
end
end
%-----------------------------------------------------------------------------------------------------------
function [new_img] = sliceresizer3(targtimg,tsmm,rsmm)
%rsmm -> Thickness of each individual slice in image1, in mm
%targtimg -> The image with slices having thickness = tsmm
%tsmm -> Thickness of each individual slice in targtimg, in mm
%output_img1 -> Resized output image, leaving out the 'stray' slices in %the last portion of the
target image volume
%
```

```
%This function resizes the slice thickness of a given target image %w.r.t a given reference image.
targt2 = sliceresizer(targtimg,tsmm); %Converts tgt to 1mm thick slices
[r1 c1 h1] = size(targt2);fac1 = mod(h1,rsmm);
%If no of stray slices is greater than half the individual slice width %then extrpolate last slice to
create a net slice of thickness = rsmm.
%If not just discard the stray slices
if fac1 >= round(rsmm/2)
for llp = 1:(rsmm-fac1)
targt2(:,:,h1+llp) = targt2(:,:,h1);
end
end
hh1 = size(targt2,3);fac2 = mod(hh1,rsmm);
arrsize = hh1-fac2;new_img = zeros(r1,c1,(arrsize/rsmm));
count=1;
for kk = 1:rsmm:arrsize
ttemp = targt2(:,:,kk:(rsmm*count));
new_img(:,:,count) = sum(ttemp,3); %Leaves out the last few slices
count = count+1;
end
%-----------------------------------------------------------------------------------------------------------
function [new_img] = sliceresizer4(targtimg,tsmm,reffimg,rsmm)
%rsmm -> Thickness of each individual slice in image1, in mm
%targtimg -> The image with slices having thickness = tsmm
%tsmm -> Thickness of each individual slice in targtimg, in mm
%output_img1 -> Resized output image, leaving out the 'stray' slices in
%the last portion of the target image volume
%
%This function resizes the slice thickness of a given target image %w.r.t a given reference image.
new_img2 = sliceresizer3(targtimg,tsmm,rsmm);
%Making equal number of slices
zee1 = size(new_img2,3);zee2 = size(reffimg,3);
if zee1 == zee2
new_img = new_img2;
elseif zee1 > zee2
new_img = new_img2(:,:,1:zee2);
else
new_img = new_img2;
for llp = 1:(zee2-zee1)
targt2(:,:,zee1+llp) = targt2(:,:,zee1);
end
end
```

# APPENDIX C

## SEGMENTATION ALGORITHMS

The program codes listed in this appendix were used to facilitate the clustering-based segmentation process. Each of these functions was used in the same order as listed below to perform the segmentation of the pancreas from the abdominal images (MR and CT).

## 1. Windowing and pre-processing function:

```
function [img2,a1,b1,a2,b2] = getsect3d(ref21,ref22,xx1,yy1,xx2,yy2)
%[Wimg,x,y,xx,yy] = getsect2_3d(img,img1,xx1,yy1,xx2,yy2)
%
%Wimg = windowed image
%x,y,xx,yy = coordinates of the diagonal of the window (useful in
%            'dispseg3d')
%img = the desired image (target image)
%img1 = the reference image
%xx1, yy1 = the coordinates of the top end point of the diagonal of the
%           window
%xx2, yy2 = the coordinates of the bottom end point of the diagonal of
the
%           window
if nargin == 2
figure; imshow(ref21(:,:,1),[]);
title('The first slice of the image volume');
%Interactively getting the required portion
counnt = 1;
while (counnt < 3)
waitforbuttonpress;
getPt = get(gca,'CurrentPoint');
crd(counnt,:) = getPt(1,1:2);
%Indicating selected points thru markers
line(crd(counnt,1),crd(counnt,2), ...
             'Marker','d', ...
             'MarkerFaceColor','g', ...
             'MarkerSize',5, ...
             'EraseMode','none');
counnt = counnt + 1;
end
xx1 = round(crd(1,1)); yy1 = round(crd(1,2));
xx2 = round(crd(2,1)); yy2 = round(crd(2,2));
elseif nargin < 6
    error('Insufficient input arguments')
end
zee1 = size(ref21,3); zee2 = size(ref22,3);
if zee1 ~= zee2
    error('Reference and Target images must be of the same size!')
end
ref21 = double(ref21); ref22 = double(ref22);
ref21 = ref21./(max(ref21(:))); ref22 = ref22./(max(ref22(:)));
%Performing the histogram equilization (slice by slice)
for i = 1:zee2
ct = imhist(ref22(:,:,i));
ttemp = ref21(:,:,i);
clear ref21(:,:,1);
ref21(:,:,i) = histeq(ttemp,ct);
end
img2 = ref21(yy1:yy2,xx1:xx2,1:zee2); %Window to section out the
pancreas
a1 = xx1; a2 = xx2; b1 = yy1; b2 = yy2;
```

## 2. Function to identify possible clusters:

```
function [hh] = clustergrp3d(img,d1,d2)
```

```
%hh = clustergrp3d(img,d1,d2)
%
%img = image for which the histogram is desired
%d1,d2 = dimensions of the gaussian filter (optional arguments)

%Default gaussian filter is 10x10
if nargin ~= 3
d1 = 10; d2 = 10;
end
h = fspecial('gaussian',[d1 d2]);
afilt = imfilter(img,h,'replicate');
afilt = afilt./(max(afilt(:)));
hh = afilt;
%Display smoothed histogram
gx = imhist(hh(:));
figure;subplot(211)
rcgx = size(gx);limt1 = max(gx(10:rcgx(1),:)) + 100;
stem(gx, 'marker', 'none');ylim([0 limt1]);
subplot(212),plot(gx(:));ylim([0 limt1]);
```

### 3. Image clustering function:

```
function [opimg, cind] = kmeanscluster3d(img,ng)
%[opimg, cind] = kmeanscluster3d(img,ng)
%
%INPUTS:
%img = image
%ng = no of groups / clusters (default = 5)
%
%OUTPUT:
%opimg = clustered image
%cind = cluster indices for each pixel
%
% This function clusters the image 'img' into 'ng' number of clusters.
The
% output clustered image 'opimg' thus has 'ng' graylevels with each
% graylevel denoting a unique cluster.

img1 = img;
imgv = img1(:); %Vectorizing the image
%Clustering using the k-means algorithm available in MATLAB
cind = kmeans(imgv,ng,'start','cluster','emptyaction','singleton');
%Reconstructing the clustered vector to obtain the clustered image
s = size(img1); imgf = zeros(s); ct = 1;
for k = 1:s(3)
for j = 1:s(2)
for i = 1:s(1)
imgf(i,j,k) = cind(ct);
ct = ct+1;
end
end
end
opimg = imgf;
```

### 4. Function to display the desired cluster:

```
function [rimg] = dispcluster3d(cimg,cno)
```

```
%rimg = dispcluster3d(cimg,cno)
%
%cimg = clustered image.. the resulting img aftr using kmeanscluster
%cno = the cluster number to be seen separately
%       (Max. upto 10 clusters only!)
%
%This function results in a black and white image displaying the
%cluster of interest alone in white and setting all the other voxels as
%background (black)
ccimg = cimg;
[s1 s2 s3] = size(ccimg);
switch cno
case 1
for k = 1:s3,for i = 1:s1,for j = 1:s2
if ccimg(i,j,k) == 1;
ccimg(i,j,k)=1;
else, ccimg(i,j,k)=0;
end
end;end;end
case 2
for k = 1:s3,for i = 1:s1,for j = 1:s2
if ccimg(i,j,k) == 2;
ccimg(i,j,k)=2;
else, ccimg(i,j,k)=0;
end
end;end;end
case 3
for k = 1:s3,for i = 1:s1,for j = 1:s2
if ccimg(i,j,k) == 3;
ccimg(i,j,k)=3;
else, ccimg(i,j,k)=0;
end
end;end;end
case 4
for k = 1:s3,for i = 1:s1,for j = 1:s2
if ccimg(i,j,k) == 4;
ccimg(i,j,k)=4;
else, ccimg(i,j,k)=0;
end
end;end;end
case 5
for k = 1:s3,for i = 1:s1,for j = 1:s2
if ccimg(i,j,k) == 5;
ccimg(i,j,k)=5;
else, ccimg(i,j,k)=0;
end
end;end;end
otherwise
error('Max 5 clusters only!');
end
rimg = ccimg;
```

## 5. Function to form the segmentation mask:

```
function [sm, imgg] = segmask3d(imgg,ch)
```

```
%sm = segmask3d(imgg)
%
%img = the respective pancreas cluster image => output image obtained
after
%       using dispcluster
%ch = either 'fill' or 'fill2'
%fill -> fills the background cylinders in the volume
%fill2 -> fills the background circles in each slice, thus giving only
          an overall outer border for segmentation
%
% This function results in a black and white mask representing the
% selected cluster
if nargin == 2
if ch == 'fill2' %slice by slice hole filling
zee = size(imgg,3);
for iu = 1:zee
imgtmp = zeros(size(imgg,1),size(imgg,2));
imgtmp2 = imgtmp; imgtmp = imgg(:,:,iu);
imgtmp2 = imfill(imgtmp,'holes');
imgg(:,:,iu) = zeros(size(imgg,1),size(imgg,2));
imgg(:,:,iu) = imgtmp2;
end
elseif ch == 'fill1' %filling the cylinders
imgg = imfill(imgg,'holes');
else
error('Invalid input argument');
end
end
[s1 s2 s3] = size(imgg);
img = imgg(1:s1,1:s2,1:s3);
img = img./(max(img(:))); %Convert to a Binary image
%Mask is obtained by dilating the image and subtracting the dilated
%image from the original image
st = strel('disk',1);
img1 = imdilate(img,st);
imask = xor(img,img1);
imask2 = imcomplement(imask);
%Draw a rectangular border around the mask
[s3 s4 s5] = size(imask2);
for k = 1:s5, for i = 1:s3
imask2(i,1,k) = 0;
imask2(i,s4,k) = 0;
end
for j = 1:s4
imask2(s3,j,k) = 0;
imask2(1,j,k) = 0;
end; end; sm = imask2;
```

## 6. Function to display the final segmented image volume:

```
function [rrimg,tar22] = dispseg3d(img,mssk,x1,y1,x2,y2)
%imagge = dispseg3d(img,msk,x1,y1,x2,y2)
%
%img = Target image / desired image
%msk = the mask obtained previously
%x1,y1,x2,y2 = the end-points of the window diagonal
%              (plug-in values %from 'getsect')
```

```
% Function to display the final segmented result
if nargin < 6
error('Missing arguments in function');
end
z = size(img,3); ref21 = double(img);
tar1 = ones(size(ref21));
tar1(y1:y2,x1:x2,1:z) = mssk; %Creates the 'bigger' version of the mask
                              %having same size as that of the image
ref22 = ref21./(max(ref21(:))); %Normalized version of input image
tar2 = ref22.*tar1;
dimg2 = ref22(y1:y2,x1:x2,1:z);
tar22 = dimg2.*mssk; %Superimposing the mask on the image
tar3 = tar2;
%Uncomment the following line if mask borders are needed to be white
%instead of black.. helps clear visualization in low contrast images
%tar3 = masker(tar2,ref22);
rrimg = tar3;
for llp = 1:size(img,3);
figure;
imshow(rrimg(:,:,llp),[]);
end
```

## REFERENCES


[1] Tortora, Gerard J., Anagnostakos, Nicholas P., *Principles of Anatomy and Physiology*, Harper & Row Publishers, New York, 1984 edition.

[2] Freelove, R., Walling, A. D., "Pancreatic cancer: Diagnosis and management", *American Family Physician*, Vol. 73, 485-492, 2006.

[3] Kalra, M. K., Maher, M. M., Mueller, P. R., Saini, S, "State-of-the-art Imaging of Pancreatic Neoplasms", *The British Journal of Radiology*, Vol. 76, pp. 857-865, 2003.

[4] Keith D. Lillemoe, M.D., "Current Management of Pancreatic Carcinoma", *Annals of Surgery*, Vol. 221, No. 2, pp. 133-148, 1995.

[5] P. A. Van den Elsen and M.A. Viergever, "Medical Image Matching - A Review with Classification", *IEEE transactions on Medical Biology,* Vol. 12, pp. 26-39, Mar. 1993.

[6] Antonie Maintz, J. B. and Max A. Viergever, "A Survey of Medical Image Registration", *Medical Image Analysis*, Vol. 2, No. 1, pp. 1-36, 1998.

[7] Woods, R. P., Grafton, S. T., Holmes, C. J., Cherry, S. R., Mazziotta, J. C., "Automated Image Registration: I. General Methods and Intrasubject, Intramodality Validation", *Journal of Computer Assisted Tomography*, Vol. 22, pp. 139-152, 1998.

[8] Josein P. W. Pluim, J.B. Antonie Maintz, Max A. Viergever, "Mutual Information Based Registration of Medical Images: A Survey", *IEEE transactions on Medical Imaging*, Vol. 22, No. 8, pp. 986-1004, Aug. 2003.

[9] Wells, W. M., Viola, P., Atsumi, H., Nakajima, S., and Kikinis, R., "Multi-Modal Volume Registration by Maximization of Mutual Information", *Medical Image Analysis*, Vol. 1, No. 1, pp. 35-51, Mar. 1996.

[10] Maes, F., Vandermeulen, D., Suetens, P., "Medical Image Registration Using Mutual Information", *Proceedings of the IEEE,* Vol. 91, No. 10, pp. 1699-1722, Oct. 2003.

[11] Li, H., Manjunath, B. S., Mitra, S. K., "A Contour-Based Approach to Multisensor Image Registration", *IEEE transactions on Image Processing*, Vol. 4, No. 3, pp. 320-334, Mar. 1995.

[12] Ventura, A., Rampini, A., Schettini, R., "Image Registration by Recognition of Corresponding Structures", *IEEE Transactions on Geoscience and Remote Sensing,* Vol. 28, pp. 305-314, 1990.

[13] Levin, D. N., Pelizzari, C. A., Chen, G. T. Y., Chen, C-T, Cooper, M. D., "Retrospective Geometric Correlation of MR, CT, and PET Images", *Radiology*, Vol. 169, pp. 817-823, 1988.

[14] Wang, X., Feng, D. D., "Automatic Hybrid Registration for 2-Dimensional CT Abdominal Images", *Proceedings of the Third International Conference on Image and Graphics (ICIG '04)*, IEEE Computer Society, 2004.

[15] Haralick, R. M., Shapiro, L. G., "Survey: Image Segmentation Techniques", *Computer Vision, Graphics and Image processing*, Vol. 29, pp. 100-132, 1985.

[16] Ball, J. E., Bruce, L. M., "Level Set Segmentation of Remotely Sensed Hyperspectral Images", *Proceedings of the IEEE international symposium on Geoscienceand Remote Sensing,* Vol. 8, pp. 5638-5642, July 2005.

[17] Kass, M., Witkin, A., Terzopoulos, D., "Snakes: Active contour models", *Proceedings of the first international conference on Computer Vision*, pp. 259-269, 1987.

[18] Williams, D. J., Shah, M., "A Fast Algorithm for Active Contours", *Computer vision and Graphics in Image Processing: Image Understanding,* Vol. 55, No. 1, pp. 14-26, 1990.

[19] Lisa G. Brown, "A Survey of Image Registration Techniques" (Project report), Department of Computer Science, Columbia University, NY, Jan. 12, 1992.

[20] Jacob Beutel (Editor), M. Sonka (Editor): *Handbook of Medical Imaging, Volume 2. Medical Image Processing and Analysis, Chapter 8: Image registration, J.M. Fitzpatrick, D.L.G. Hill and C.R. Maurer*, SPIE Press Monograph.

[21] Derek L. G. Hill, Philipp G. Batchelor, Mark Holden, David J. Hawkes, "Medical Image Registration", *Physics in Medicine and Biology*, No. 46, R1-R45, 2001.

[22] Collignon, D., Maes, F., Vandermeulen, D., Marchal G. and Suetens, P., "Multi-modality Image Registration by Maximization of Mutual Information", *IEEE Transactions on Medical Imaging,* Vol. 16, pp. 187-198, Apr. 1997.

[23] Nelder, J. A. and Mead, R,"A Simplex Method for Function Minimization." *Computer Journal*, Vol. 7, pp. 308-313, 1965.

[24] Studholme, C., Hill, D. L. G., Hawkes, D. J., "An Overlap-invariant Entropy Measure of 3D Medical Image Alignment", *Pattern Recognition*, Vol. 32, No. 1, pp. 71-86, 1999.

[25] William H. Press, Saul Teukolsky, William T. Vetterling, Brian P. Flannery, *"Numerical Recipies in C: The art of scientific computing"*, Chapter 10, pp. 408-430, Cambridge University Press, Second edition, 1997.

[26] Mistry, N. M. and Hsu, E. W., "Retrospective Distortion Correction For 3D MR Diffusion Tensor Microscopy using Mutual Information and Fourier Deformations", *Magnetic Resonance in Medicine*, Vol. 56, pp. 310-316, 2006.

[27] Kanungo, T., Mount, D. M., Netanyahu, N. S., Piakto, C. D., Silverman, R., Wu, A. Y., "An Efficient k-means Clustering Algorithm: Analysis and Implementation", *IEEE transactions on pattern analysis and machine intelligence*, Vol. 24, No. 7, pp. 881-892, Jul. 2002.

[28] Coleman, G. B., Andrews, H. C., "Image Segmentation by Clustering", *Proceedings of the IEEE*, Vol. 67, No. 5, pp. 773-785, May 1979.

[29] Haralick, R. M., Dinstein, I., "A Spatial Clustering Procedure for Multi-image Data", *IEEE transactions on circuits and systems*, Vol. cas-22, No. 5, pp. 440-450, May 1975.

[30] Cheung, Y-M., "$k^*$-means: A New Generalized k-means Clustering Algorithm", *Pattern Recognition Letters*, Vol. 24, No. 15, pp. 2883-2893, Apr. 2003.

[31] Haralick., R. M., Kelly, G. L., "Pattern Recognition with Measurement Space and Spatial Clustering for Multiple Images", *Proceedings of the IEEE*, Vol. 57, No. 4, pp. 654-665, Apr. 1969.

[32] Jain, A. K., Murthy, M. N., Flynn, P. J., "Data Clustering: A review", *ACM Computing Surveys*, Vol. 31, No. 3, Sep. 1999.

[33] Teknomo, Kardi, "K-Means Clustering Tutorials", *http:\\people.revoledu.com\kardi\ tutorial\kMean*

[34] MacQueen, J., "Some Methods for Classification and Analysis of Multivariate Observations", *Proceedings of the Fifth Berkeley Symposium on Mathematical Statistics and Probability*, Vol. 1, pp. 281-296, Berkeley, CA, 1967.

[35] Josein P. W. Pluim, J.B. Antonie Maintz, Max A. Viergever, "Interpolation Artifacts in Mutual Information-based Image Registration", *Computer Vision Image Understanding*, Vol. 77, pp. 211-232.

[36] http://www.cancerbackup.org.uk/content/images/ (Cited on Date: 04/20/2007)